Inorganic Chemistry

Article

pubs.acs.org/IC

Thiocyanate Complexes of Uranium in Multiple Oxidation States: A Combined Structural, Magnetic, Spectroscopic, Spectroelectrochemical, and Theoretical Study

Emtithal Hashem,[†] James A. Platts,[‡] František Hartl,[§] Giulia Lorusso,[∥] Marco Evangelisti,[∥] Carola Schulzke,[⊥] and Robert J. Baker*[,†]

[†]School of Chemistry, University of Dublin, Trinity College, College Green, Dublin 2, Ireland

[‡]School of Chemistry, Cardiff University, Main Building, Park Place, Cardiff CF10 3AT, United Kingdom

[§]Department of Chemistry, University of Reading, Whiteknights, Reading, RG6 6AD, United Kingdom

[∥]Departamento Física Materia Condensada, Instituto de Ciencia de Materiales de Aragón (ICMA), CSIC-Universidad de Zaragoza, Zaragoza 50009, Spain

[⊥]Institut für Biochemie, Ernst-Moritz-Arndt Universität Greifswald, Felix-Hausdorff-Strasse 4, D-17487 Greifswald, Germany

Supporting Information

ABSTRACT: A comprehensive study of the complexes $A_4[U(NCS)_8]$ (A = Cs, Et_4N, $^nBu_4N$) and $A_3[UO_2(NCS)_5]$ (A = Cs, Et_4N) is described, with the crystal structures of $[^nBu_4N]_4[U(NCS)_8]\cdot 2MeCN$ and $Cs_3[UO_2(NCS)_5]\cdot O_{0.5}$ reported. The magnetic properties of square antiprismatic $Cs_4[U(NCS)_8]$ and cubic $[Et_4N]_4[U(NCS)_8]$ have been probed by SQUID magnetometry. The geometry has an important impact on the low-temperature magnetic moments: at 2 K, μ_{eff} = 1.21 μ_B and 0.53 μ_B, respectively. Electronic absorption and photoluminescence spectra of the uranium(IV) compounds have been measured. The redox chemistry of $[Et_4N]_4[U(NCS)_8]$ has been explored using IR and UV−vis spectroelectrochemical methods. Reversible 1-electron oxidation of one of the coordinated thiocyanate ligands occurs at +0.22 V vs Fc/Fc^+, followed by an irreversible oxidation to form dithiocyanogen $(NCS)_2$ which upon back reduction regenerates thiocyanate anions coordinating to UO_2^{2+}. NBO calculations agree with the experimental spectra, suggesting that the initial electron loss of $[U(NCS)_8]^{4-}$ is delocalized over all NCS^- ligands. Reduction of the uranyl(VI) complex $[Et_4N]_3[UO_2(NCS)_5]$ to uranyl(V) is accompanied by immediate disproportionation and has only been studied by DFT methods. The bonding in $[An(NCS)_8]^{4-}$ (An = Th, U) and $[UO_2(NCS)_5]^{3-}$ has been explored by a combination of DFT and QTAIM analysis, and the U−N bonds are predominantly ionic, with the uranyl(V) species more ionic that the uranyl(VI) ion. Additionally, the U(IV)−NCS ion is more ionic than what was found for U(IV)−Cl complexes.

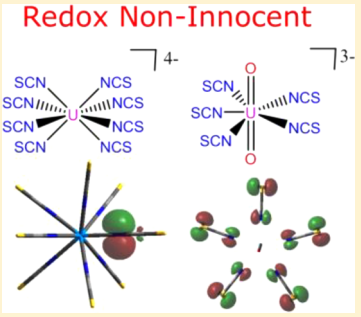

INTRODUCTION

The coordination and organometallic chemistry of the actinides (An) is undergoing a resurgence in interest, and new reactivity patterns, most notably in molecular uranium chemistry, are being uncovered that challenge understanding of how the 5f and 6d orbitals are involved in bonding to ligands.[1] Uranium(III) compounds have been extensively explored since new precursors for this oxidation state have been developed,[2] and the small molecule activation of compounds in this oxidation state has been nothing short of outstanding.[3] Uranyl(V)[4] and uranyl(VI)[5] chemistry, $[UO_2]^{n+}$, has also developed at an unprecedented rate, and new chemistry is being reported that enhances our knowledge of these species. Arguably the most impressive recent results are the synthesis of uranium(II) complexes from the Evans[6] and Meyer[7] groups or successful isolation of elusive terminal nitrides of uranium(V)[8] and uranium(VI)[9] which illustrates the vibrancy of the field of actinide science.

The evidence for enhanced covalency in an An−L bond compared to the corresponding Ln−L (Ln = lanthanides) bond has the potential to form the basis for advanced nuclear fuel cycles.[10] Of the methods currently under investigation, ionic liquids appear to hold particular promise.[11] This topic has been intensively explored using a plethora of experimental and theoretical methods as the chemistry underpinning this separation science is essential to elucidate. One experimental technique that shows promise for elucidation of the electronic structure of an actinide ion is photoluminescence spectroscopy,[12] although this is not as well developed as for lanthanide ions. Uranyl(VI) emission is the most studied, and the green emission is due to de-excitation of formally triplet ligand-to-metal charge-transfer ($^3\Pi_u$) excited states. Recent results indicate that this can be used to study the structural and electronic features of air- and moisture-sensitive coordination complexes.[13] In certain laboratories, Am(III) and Cm(III) time-resolved laser-induced emission spectroscopy has been used to conveniently characterize low concentrations of

Received: May 28, 2014
Published: July 29, 2014

   dx.doi.org/10.1021/ic501236j | Inorg. Chem. 2014, 53, 8624−8637

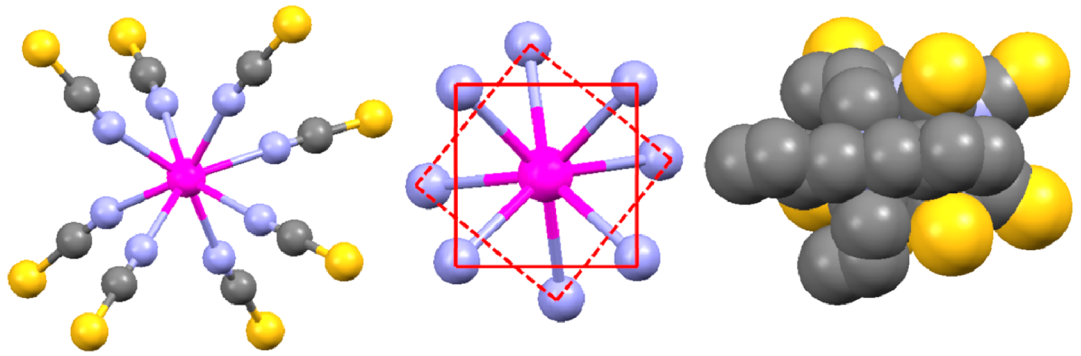

Figure 1. Solid-state structure of the anion of $[^nBu_4N]_4[\mathbf{1}]\cdot 2MeCN$ (left); coordination geometry of the uranium center (middle); space-filling diagram showing the interaction of one cation with the anion (right). Average bond lengths (Å): U−N = 2.430; N═C = 1.167; C═S = 1.628.

these highly radioactive isotopes.[12a,14] We recently reported on the use of photoluminescence spectroscopy to fingerprint the U(IV) oxidation state.[15] From our studies and the reported photoluminescence spectra of the hydrated U(IV) ion,[16] we can suggest that de-excitation occurs from a charge-transfer band (the $5f^1$ $6d^1$ charge-transfer excited-state manifold in simple uranium halide complexes) or the highest energy $^1S_0$ Russell−Saunders coupled state (in the hydrated ion) to lower lying $5f^2$ spin−orbit coupled levels. Computational studies on the hydrated ion indicate that when the highest energy term is corrected for a large Stokes shift (i.e., solvation effects), the assignment of the emission bands changes considerably.[17] We have therefore become interested in the pseudohalide complex $[U(NCS)_8]^{4-}$, as the high symmetry will allow the influence of the geometry on the photoluminescence properties to be explored. The uranium(IV) thiocyanate complex $[Et_4N]_4[U(NCS)_8]$ was prepared in the 1960s[18] and structurally characterized in 1971. It has a cubic geometry around the uranium metal ion,[19] while the corresponding Cs^+ salt is square-antiprismatic.[20] However, both salts in solution show the same geometry, namely, square antiprismatic, based on ^{13}C NMR and vibrational spectroscopic data.[21] Moreover, the thiocyanate ligand can be used in liquid−liquid extractions[11] or as a component of ionic liquids, aimed at separating the actinides from the lanthanides[22] for advanced fuel cycles. [A336][SCN] (A336 = tricaprylmethylammonium) is a task-specific ionic liquid of sufficiently low viscosity to be used without utilizing a separate extractant, and substantial distribution ratio enhancements have been reported, although the mechanism is unknown.[23] Toward this goal, spectroscopic characterization of the uranyl thiocyanate[24] $[UO_2(NCS)_5]^{3-}$ in ionic liquids[25] has been reported, and some recent structural and Raman spectroscopic data[26] have shed light on these species.

In this contribution we fully explore the chemistry of uranium thiocyanates in the +4 and +6 oxidation states using a suite of spectroscopic and computational measurements. A spectroelectrochemical investigation of the redox nature of $[Et_4N]_4[U(NCS)_8]$ will be reported, and a comprehensive computational study allows the bonding to be analyzed in detail.

RESULTS AND DISCUSSION

Structural and Spectroscopic Studies of $[A]_4[U^{IV}(NCS)_8]$ [1] (A = Et_4N^+; $^nBu_4N^+$, Cs^+). Structural studies carried out in the 1970s showed that the Et_4N^+ cation appeared to template the geometry of the $[An^{IV}(NCS)_8]^{4-}$ anion (An = Th, Pa, U, Np, Pu), so that a cubic symmetry was favored, while the Cs^+ salts (An = Th, U) preferred a square-antiprismatic geometry. This was postulated to be due to the crucifix-type geometry of the cation packing against a cubic face of the anion. The small energy difference between the two geometries must therefore be governed by crystal packing effects. Changing the tetraethylammonium counterion to the longer $^nBu_4N^+$ might be expected to give a lower symmetry and may shed light on the uranium coordination in ionic liquids using long-chain tetraalkyl ammonium cations. Moreover, as a number of our spectroscopic measurements have been conducted in the presence of tetra-*n*-butyl ammonium cations, it is important to ascertain their influence on the structure. Accordingly, we prepared and structurally characterized $[^nBu_4N]_4[U(NCS)_8]$, $[^nBu_4N]_4[\mathbf{1}]$, as shown in Figure 1. The U−N bond distances range from 2.402(4) to 2.460(4) Å with the average (2.43 Å) being close to that observed for $[Et_4N]_4[\mathbf{1}]$ (2.38 Å) and $Cs_4[\mathbf{1}]$ (2.42 Å). The average bond lengths for N═C and C═S being 1.167 and 1.628 Å, respectively, are also very close to the average bond lengths in $[Et_4N]_4[\mathbf{1}]$ and $Cs_4[\mathbf{1}]$ (N═C 1.14 Å and C═S 1.61 Å for $[Et_4N]_4[\mathbf{1}]$ and N═C 1.145 Å and C═S 1.60 Å for $Cs_4[\mathbf{1}]$). The geometry around the uranium and the subsequent packing of the anion are different. The less rigid butyl arms wrap around the voids in the uranium coordination sphere and cause the U−N−C angle to bend to 165°, and the geometry is best described as a distorted square antiprism (interplane N−U−N angles = 73−85°). Raman and infrared spectra of $[^nBu_4N]_4[\mathbf{1}]$ in both the solid state and solution are identical to those of $Cs_4[\mathbf{1}]$, confirming the coordination geometry.

Early reports on the synthesis of these thiocyanate species stated that the compounds were sensitive to air and moisture, and the hydrated compound $[U(NCS)_4(H_2O)_4(18\text{-crown-}6)]$[27] has been structurally characterized. We noted that $[A]_4[\mathbf{1}]$ (A = Cs^+, Et_4N^+) is stable in air as a solid for a number of days and can be recrystallized from acetonitrile in air without decomposition. When $[A]_4[\mathbf{1}]$ is treated with THF, in which it is almost insoluble, a slow reaction occurs and an orange solution is formed. Interestingly, the orange solution deposits orange crystals when recrystallized in daylight; in the dark, the original green crystals are recovered. The orange crystalline material has identical vibrational spectra to $[A]_4[\mathbf{1}]$, and a single-crystal X-ray structural determination for A = Et_4N^+ shows that this orange material has the same cell and metric parameters as the green $[Et_4N]_4[\mathbf{1}]$ (Tables S1−S3, Supporting Information). This suggests that $[A]_4[\mathbf{1}]$ is photochemically sensitive, so we examined the changes in the UV−vis spectrum upon irradiation with UV light (λ_{ex} = 340 nm; Figure 2) under an inert atmosphere. The initial UV−vis spectrum of $[Et_4N]_4[\mathbf{1}]$ in MeCN displays one intense band centered at 233 nm, and upon irradiation new bands at 276 (ε = 7600 M^{-1} cm^{-1}) and 340 nm (ε = 1800 M^{-1} cm^{-1}) grow in over time; the molar

dx.doi.org/10.1021/ic501236j | Inorg. Chem. 2014, 53, 8624−8637

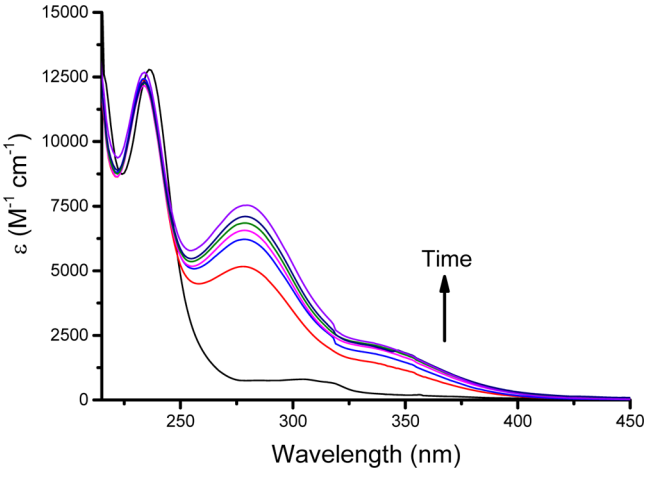

Figure 2. Changes in the UV−vis spectrum of $[Et_4N]_4[\mathbf{1}]$ in MeCN upon exposure to UV light (λ_{exc} = 340 nm) measured over 3 h.

absorption coefficient of the former suggests a charge transfer band. When this sample is allowed to stand in the dark, the original spectrum is recovered. Thermochromic behavior has been reported previously for $[C_4mim]_x[UO_2(NCS)_y]$ (C_4mim =1-butyl-3-methylimidazolium; x = 1−4, y = 3−6) in ionic liquids whereby dissociation of a thiocyanate ligand was postulated as an explanation,[25] while a number of studies on the photochemical activation of chromium complexes such as Reinecke's salt affords some of the long-lived (hundreds of microseconds) dimeric radical anion $[(NCS)_2]^{\bullet-}$, formed by dissociation and identifiable by a characteristic maximum at 480−490 nm.[28] In our system we see no evidence of dissociation by vibrational spectroscopy, and the peak positions in the IR spectrum do not change. This eliminates the possibility of linkage isomerization,[29] and there is no evidence for a uranyl stretch in the IR spectrum, which excludes oxidation of the complex. In addition, no evidence of metal-based redox reactions is observed as judged by SQUID magnetometry on "green" and "orange" $Cs_4[\mathbf{1}]$ (Figure 3). The corresponding thorium(IV) complex

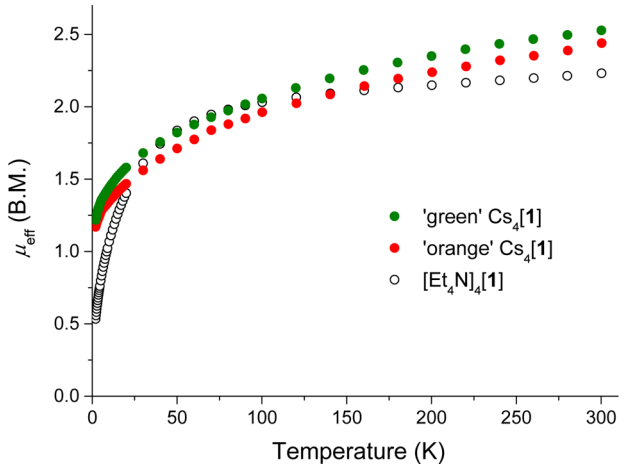

Figure 3. Magnetic susceptibility measurements, collected at 0.1 T for $[Et_4N]_4[\mathbf{1}]$ (empty circles), "green" $Cs_4[\mathbf{1}]$ (green), and "orange" $Cs_4[\mathbf{1}]$ (red).

$[Et_4N]_4[\mathbf{2}]$ also undergoes this photochemistry to give the same spectroscopic features. Moreover, both $[Et_4N]_4[\mathbf{1}]$ and $[Et_4N]_4[\mathbf{2}]$ were found to be EPR inactive after UV irradiation. We are unsure as to the molecular interpretation for this reversible behavior.

Recent interest in uranium chemistry has come from the magnetic properties,[30] in particular as a number of compounds show single-molecule magnetic (SMM) behavior. For example, the U(III) species $[U(Ph_2BPz_2)_3]$,[31] $[U(H_2BPz_2)_3]$,[32] $[U(Tp)_3]$,[33] $[U(Tp^*)_2I]$,[34] $[U(Tp^*)_2(bipy)]I$,[35] $[(U(BIPM^{TMS}H)(I))_2(\mu\text{-}\eta^6\text{:}\eta^6\text{-PhMe})]$,[36] and $[U^VO_2]^+$ complex $[\{[UO_2(salen)]_2Mn(Py)_3\}_6]$[37] all show SMM behavior (Py = pyridine; Pz = pyrazolyl; Tp = tris(pyrazolyl)borate; Tp* = hydrotris(3,5-dimethylpyrazolyl)borate; $BIPM^{THS}H$ = $HC(PPh_2NSiMe_3)_2$; $salenH_2$ = *N*,*N*′-ethylenebis(salicylimine)). Most interestingly, it appears that the SMM behavior is an intrinsic property of U(III).[38] Uranyl(V) single-ion magnets[39] and uranyl(V)−Mn(II)[40] single-chain magnets have also been reported. A recent computational study[41] has suggested that also U(IV) compounds could show unusual magnetic behavior, particularly in tetragonal or trigonal prismatic geometries with ground states $M_J = \pm 3$ or $M_J = \pm 4$. We explored the magnetic properties of $Cs_4[\mathbf{1}]$ and $[Et_4N]_4[\mathbf{1}]$ as shown in Figure 3. Variable-temperature magnetic susceptibility of $[Et_4N]_4[\mathbf{1}]$ is typical of U(IV) within a region of temperature-independent paramagnetism (μ_{eff} at 300 K = 2.23 μ_B) followed by a precipitous drop at low temperatures (μ_{eff} at 2 K = 0.53 μ_B), consistent with a singlet ground state. However, there is a striking difference to the magnetic profile of $[Cs]_4[\mathbf{1}]$ at low temperatures (μ_{eff} at 2 K = 1.21 μ_B). Variable field (Figure S1, Supporting Information) and ac susceptibility measurements (Figure S2, Supporting Information) corroborate the +4 oxidation state, so we believe this difference must be due to the change in geometry, as the solid-state structures show no evidence of close contacts between uranium molecules. The ac susceptibility shows no unusual behavior, suggesting that in our examples at least the ground state is not conducive for the SMM behavior. It is worth noting that this is the first study on the geometry dependence upon the magnetic susceptibility with the same ligand set. From these results it is clear that small changes in geometry can have a drastic change in the ground state configuration; we are exploring this in more detail and will report on our results in due course.

Photoluminescence Spectroscopy. Our interest in $[A]_4[\mathbf{1}]$ was initially to explore the photoluminescence properties of these complexes. In order to understand the photoluminescence spectra, we first sought to fully assign the electronic absorption spectrum. The open-shell nature of these compounds makes the assignment of absorption and emission bands challenging, although analysis based upon the Russell−Saunders coupling scheme can be used as a good approximation.[14b] The electronic absorption spectrum of $[Et_4N]_4[\mathbf{1}]$ in MeCN is shown in Figure 4; that of the corresponding $Cs_4[\mathbf{1}]$ is identical. There is one intense band in the UV region (λ_{max} = 230 nm, ε = 13 700 M^{-1} cm^{-1}) that can be assigned to ligand-based n−π^* bands, as they are also observed in the thorium analogue, $[Et_4N]_4[\mathbf{2}]$, and in Na[NCS]. Interestingly the f−d transition is not observed in this case, so the excited state must lie higher than 45 450 cm^{-1} above the ground state; in $[Li(THF)_4][UCl_5(THF)]$ the corresponding transition was found at 36 100 cm^{-1}.[15] The weak bands in the visible and near-infrared regions are assigned to intraconfigurational f−f transitions, and the low molar absorption coefficients (ε = 20−200 M^{-1} cm^{-1}) are likely due to the high symmetry of this complex. We have recently shown that the local geometry and crystal field effects are rather unimportant in the energy of the f−f transitions,[15] so we assigned the spectrum of $[Et_4N]_4[\mathbf{1}]$ based upon published theoretical treatment of $[U(H_2O)_8]^{4+}$ using CASPT2 techniques.[17] Assignments shown in Figure 4 are the

dx.doi.org/10.1021/ic501236j | Inorg. Chem. 2014, 53, 8624−8637

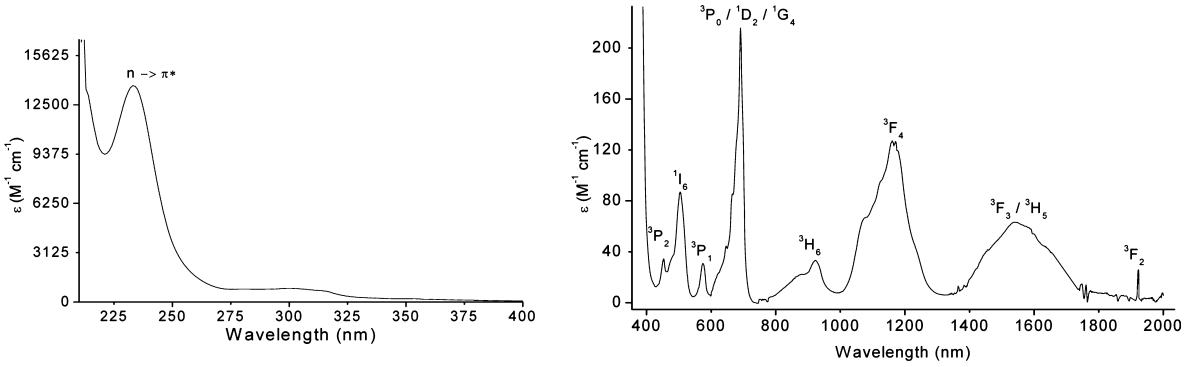

Figure 4. UV (left) and vis–NIR (right) absorption spectrum of $[Et_4N]_4[\mathbf{1}]$ in MeCN.

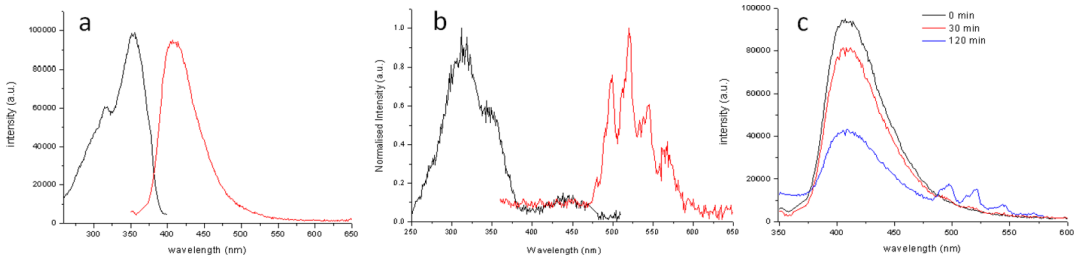

Figure 5. Excitation (black) and emission (red) spectra of (a) $[Et_4N]_4[\mathbf{1}]$ (λ_{ex} = 340 nm; λ_{em} = 420 nm) and (b) $[Et_4N]_3[UO_2(NCS)_5]$ (λ_{ex} = 340 nm and λ_{em} = 520 nm), and (c) emission spectra of $[Et_4N]_4[\mathbf{1}]$ exposed to air (λ_{ex} = 340 nm), all at 298 K in CD_3CN.

transitions from the Russell–Saunders coupled $^3H_4$ ground state to the states of higher energy; the transition to the highest energy $^1S_0$ state is presumably buried under the intense ligand-based bands in the UV region. Interestingly, in comparison to $[Et_4N][U(NCS)_5(bipy)_2]$ and $[Li(THF)_4][UCl_5(THF)]$ there is little difference in the position of these bands (Table S4, Supporting Information).

Attempts to obtain a photoluminescence spectrum of $[Et_4N]_4[\mathbf{1}]$ by excitation into any of the absorption bands in MeCN gave no detectable signal. This may be due to the high symmetry, which means the oscillator strengths of the bands are small. However, repeating the measurements in CD_3CN does give a photoluminescence spectrum, which is shown in Figure 5a. A broad, weak band centered at 410 nm is consistent with our observations on the uranium halide complexes, and the measured lifetime is 10 ns. Using the absorption spectra we can postulate that excitation into the ligand chromophore is followed by inefficient electron transfer and subsequent de-excitation through the f-orbital manifold; this is similar to our recent studies on $[UX_5(THF)]^-$ whereby excitation occurred into the d orbitals. As the emission profile is broad it is likely that the observed emission terminates in an envelope of energy levels. Essentially we are using an "antenna" effect to sensitize the emission of the U(IV) complex, which is reminiscent of lanthanide photoluminescence spectroscopy. We were unable to measure the quantum yield for $[Et_4N]_4[\mathbf{1}]$ as the emission is weak, but the emission intensity is comparable to that of the Raman bands in this solvent. In order to eliminate the possibility of observing a uranyl impurity we conducted two additional experiments. First, an authentic sample of $[Et_4N]_3[U^{VI}O_2(NCS)_5]$ was prepared (electronic absorption spectra can be found in Figure S3, Supporting Information)[26] and measured in both CH_3CN and CD_3CN, which gave vibronically coupled bands centered at 520 nm (E_{0-0} = 20 040 cm^{-1}) with a lifetime of 1.4 μs in CD_3CN (Figure 5b); the vibronic progressions that correspond to the ν_1 and ν_2 vibrational modes (890 cm^{-1}) match reasonably well with those determined from the Raman spectra (850 cm^{-1}). This spectrum is essentially identical to that observed of this anion in ionic liquids.[25] Second, $[Et_4N]_4[\mathbf{1}]$ was exposed to air and the emission monitored over time. The decay in intensity of the band at 400 nm and the increase in intensity of the vibronically coupled bands centered at 500 nm prove conclusively the observation of U(IV) (Figure 5c). Further evidence for the involvement of f orbitals in the emission is that no emission was seen from the corresponding thorium complex, $[Et_4N]_4[\mathbf{2}]$, with the f orbitals lying much higher in energy,[42] or Na[NCS] under identical conditions.

Most U(IV) compounds contain ligands that have low-lying charge transfer absorptions that can mask f–f transitions and allow different decay processes to occur upon excitation. This is exemplified by the reports of the metallocene ketimide system $[Cp^*_2U\{N{=}C(Ph)(CH_2Ph)\}_2]$ ($Cp^* = C_5Me_5$), where no 5f-centered emission was observed following photoexcitation. Decay from the ligand-centered singlet state proceeds directly through the 5f-electron manifold, resulting in efficient quenching of the emission and lifetimes of picosecond order.[43] Therefore, on the basis of our studies we can postulate that uranium(IV) compounds that do not have ligand-centered CT bands in the visible region of the spectra may show photoluminescent behavior. We are currently exploring this thesis in detail.

DFT Studies on the Bonding in $[\mathbf{1}]^{4-}$. In order to gain further insight into the electronic structure of the studied compounds, especially the degree of covalency of the U–N bonds, which may be important in Ln/An differentiation in ionic liquids, we turn to density functional theory (DFT) that is increasingly being utilized in this field.[44] Geometry optimization of triplet $[U(NCS)_8]^{4-}$ using both pure (BP86) and hybrid (B3LYP) functionals with a TZVPP basis set resulted in square-antiprismatic geometry, with the point group D_{4d}, confirmed as an energy minimum by harmonic frequency calculation. A comparison

dx.doi.org/10.1021/ic501236j | Inorg. Chem. 2014, 53, 8624–8637

Table 1. DFT Geometry and Vibrational Modes Using the BP86 and B3LYP Basis Sets, and Experimental Values for $Cs_4[1]$ and $[Et_4N]_4[2]$

	bond lengths (Å)			N−C stretch (cm^{-1})		C−S stretch (cm^{-1})	
	U−N	N−C	C−S	IR	Raman	IR	Raman
$[1]^{4-}$							
expt	2.38(3) 2.46(3)	1.15(4) 1.14(4)	1.63(4) 1.61(3)	2047	2045	783	823
				2090	2055	786	810
					2090		
BP86	2.469	1.185	1.644	2067 (b_2)	2057 (e_2)	797	805
				2071 (e_1)	2060 (e_3)		
					2099 (a_1)		
B3LYP	2.485	1.171	1.644	2151 (b_2)	2139 (e_2)	803	811
				2154 (e_1)	2144 (e_3)		
					2191 (a_1)		
$[2]^{4-}$							
expt[a]	2.47(2)	1.15(2)	1.59(2)				
BP86	2.538	1.185	1.644	2072	2107	800	809

[a]For $[Et_4N]_4[Th(NCS)_8]$.

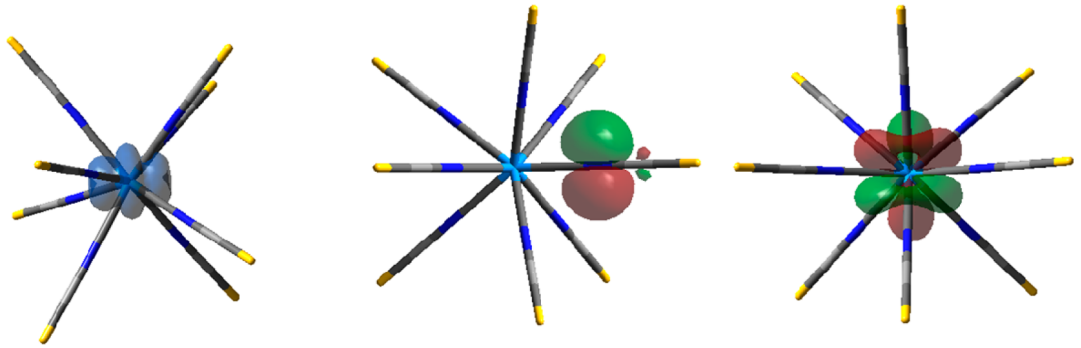

Figure 6. Spin density (left), HOMO (middle), and LUMO (right) of $[1]^{4-}$ at the BP86 level of theory.

between the calculated and the experimentally determined bond lengths and angles for the square-antiprismatic $Cs_4[1]$ is reported in Table 1. DFT geometries generally reproduce the solid-state geometry well; however, geometry optimization of isolated tetra-anion $[1]^{4-}$ results in exactly linear NCS groups, supporting the observation that the nonlinearity of these groups in the solid state is due to crystal packing forces.

Previous DFT studies of actinide complexes reported significant differences in the description of metal−ligand bonding between pure and hybrid DFT methods. Table 1 indicates that BP86 reproduces the X-ray U−N and C−S bond lengths within an experimental error but significantly overestimates the N−C length. In contrast, B3LYP overestimates the U−N and N−C bond lengths. Given the apparent importance of crystal packing, it is not possible to deduce from this data whether one method gives a better description of bonding. Instead, the vibrational modes of the NCS group, especially the N−C stretching modes, allow a more reliable test of the performance of these methods. Not only is this mode easily observed in IR and Raman spectra, but it should also be sensitive to the electronic character of the U−N bonding. Table 1 clearly shows that BP86 yields a much better description of this mode than does B3LYP.[45] Two bands due to IR-active modes are found within 20 cm^{-1} of the experimental value, while the most intense Raman bands are centered at 2060 cm^{-1}, again slightly above the experimental value, with a less intense peak close to the experimental band at 2093 cm^{-1}. In contrast, B3LYP overestimates the energy of these bands by as much as 100 cm^{-1}.

Since BP86 gave the most appropriate fit to the experiment, we utilized this method to examine the bonding in $[1]^{4-}$ and related compounds. This method has found that the HOMO is ligand based, and the LUMO is of 5f-orbital character (Figure 6). The calculated HOMO−LUMO gap is 17 905 cm^{-1} (17 018 cm^{-1} for the β-spin), and the d orbitals are ∼44 000 cm^{-1} higher in energy than the ground state; experimentally the d orbitals are higher than 50 000 cm^{-1}. Natural bond order (NBO) analysis finds a single bonding orbital for each U−N bond (Figure 7), made up of 10.9% U and 89.1% N character, of which the U orbital contribution is 12.34% s, 34.14% p, 38.01% d, and 15.51% f. This can be compared to the U−Cl bond in $[UCl_5(THF)]^-$ (17% U and 83% Cl; 20% s, 26% p, 41% d and 14% f).[15] This analysis also locates one σ- and two π-bonding orbitals in N−C and a single σ C−S bond, suggesting that the most appropriate resonance form of the coordinated thiocyanate ligand is $[N{\equiv}C{-}S]^-$ with lone pairs of electrons on the sulfur, which may be accessible for bonding to soft transitional metals. NBO indicates a charge on U in $[1]^{4-}$ of just +0.26, much less than the formal charge of +4, with corresponding charges of −0.18, +0.07, and −0.16 on N, C, and S, respectively. For comparison, data for $[2]^{4-}$ indicates slightly longer Th−N bonds than in the U complex but identical N−C and C−S metric parameters and vibrational data, the charge of +1.20 on Th pointing to a much higher contribution of ionic bonding in this complex. It should be noted that experimental bond lengths for $Cs_4[2]$ are unavailable. However, the cubic $[Et_4N]_4[2]$ has been structurally characterized, and despite the different geometry, it follows the same trend as for $Cs_4[1]$.

dx.doi.org/10.1021/ic501236j | Inorg. Chem. 2014, 53, 8624−8637

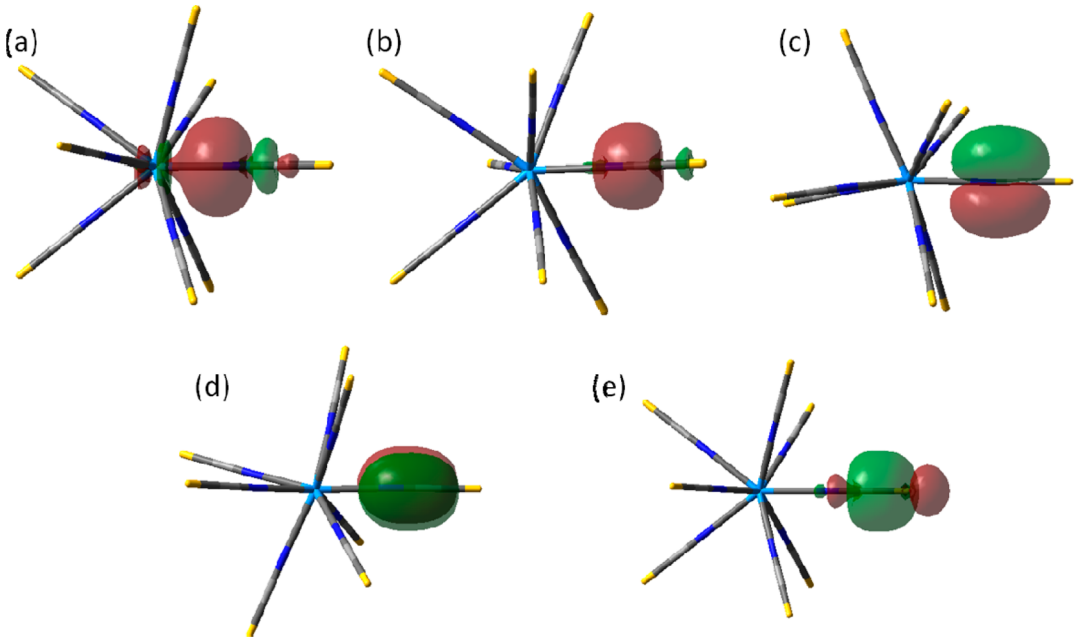

Figure 7. NBO analysis for $[\mathbf{1}]^{4-}$: (a) U−N σ NBO; (b) N−C σ NBO; (c and d) degenerate N−C π NBO; (e) C−S σ NBO.

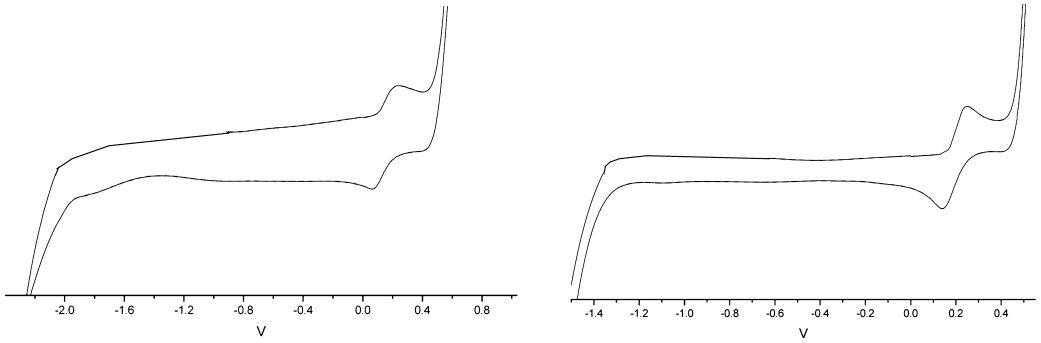

Figure 8. CV of complexes $[Et_4N]_4[\mathbf{1}]$ (left) and $[Et_4N]_4[\mathbf{2}]$ (right) vs Fc/Fc^+ in THF at 293 K, with ~0.1 M $[Bu_4N][BPh_4]$ as the supporting electrolyte (scan rate = 0.1 V s^{-1}).

Table 2. Selected Redox Couples for Uranium(IV) and Thorium(IV) Complexes

	E/V vs Fc/Fc^+		
complex	An(IV)/An(III)	An(IV)/An(V)	ref
$[Et_4N]_4[\mathbf{1}]$	−1.8	+0.22(ligand based)	this work
$[Et_4N]_4[\mathbf{2}]$		+0.22 (ligand based)	
$(C_5Me_5)_2UCl_2$	−1.85		47
$(C_5Me_5)_2U(CH_3)_2$	−2.41		48
$(C_5Me_5)_2U(\eta^2(N,N')\text{-}CH_3NN{=}CPh_2)(SO_3CF_3)$	−2.01	+0.18	49
$(C_5Me_5)_2U[\eta^2(N,N')\text{-}CH_3NN{=}CPh_2]_2$	−2.78	−0.68	
$(C_5Me_5)_2U[-N{=}C(Ph)_2]_2$	−2.50	−0.48	
$(C_5Me_5)_2Th[\eta^2(N,N')\text{-}PhNN{=}CPh_2]_2$	−3.0		
$(C_5Me_5)_2Th[-N{=}C(Ph)_2]_2$	−2.8		

All complexes of this family have the same resonance structure of one U/Th−N, three N−C, and one C−S bonding orbitals.

Electrochemical and Spectroelectrochemical Studies. To corroborate the nature of the ligand-based HOMO (Figure 6), we measured the cyclic voltammogram of $[Et_4N]_4[\mathbf{1}]$ and $[Et_4N]_4[\mathbf{2}]$ (Figure 8).

For $[Et_4N]_4[\mathbf{1}]$ there is a broad irreversible cathodic wave at $E_{p,c} = -1.80$ V which may be ascribed to a U(III)/U(IV) couple, in line with other examples in the literature (Table 2). Further, there is a reversible oxidation at $E_{1/2} = +0.22$ V that could be assigned formally as a U(IV)/U(V) redox couple or, as predicted by DFT, as a ligand-based couple. In the cyclic voltammogram of $[Et_4N]_4[\mathbf{1}]$ measured in MeCN (Figure S4, Supporting Information) the reversible oxidation at $E_{1/2} = +0.22$ V is electrochemically quasi-reversible, possibly due to surprisingly slow electron transfer kinetics as the internal standard was not influenced, and there is an appearance of second, irreversible oxidation at $E_{p,a=}$ +0.52 V. It is known that oxidation of ionic liquids with

dx.doi.org/10.1021/ic501236j | Inorg. Chem. 2014, 53, 8624−8637

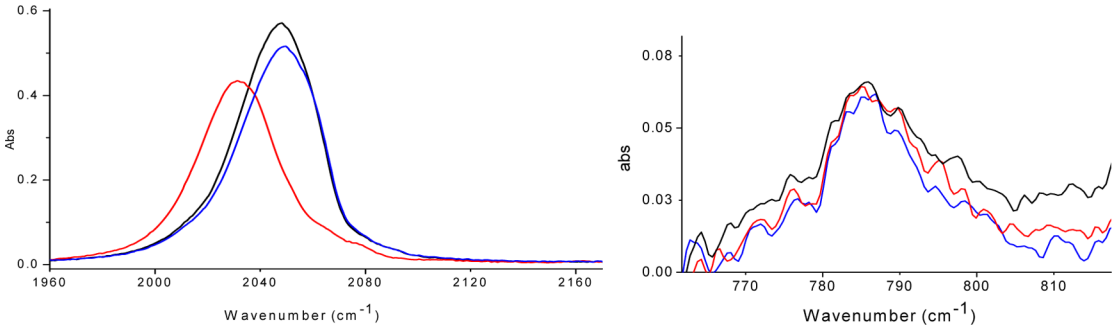

Figure 9. IR spectral changes in the ν(C═N) region (left) and ν(C═S) region (right), accompanying the reversible 1e$^-$ oxidation of $[\mathbf{1}]^{4-}$ to stable $[\mathbf{1}]^{3-}$ in acetonitrile/$[^nBu_4N][PF_6]$ at 293 K within an OTTLE cell. Spectra: black, before oxidation; red, after oxidation at +0.22 V; blue, after reversible back reduction.

$[NCS]^-$ counterions has a limited anodic window due to the irreversible oxidation of $[NCS]^-$ to thiocyanogen, NCS−SCN ($E_{p,a}$ = +0.42 V vs Fc/Fc$^+$),[46] but this does not correspond with the redox couple in $[Et_4N]_4[\mathbf{1}]$. In order to fully assign these anodic waves we first also explored the electrochemistry of the thorium analogue, $[Et_4N]_4[\mathbf{2}]$, which would not have an accessible metal-based oxidation. The cyclic voltammogram of this complex (Figure 8) shows no reduction wave within our experimentally accessible window but again the same oxidation wave at $E_{1/2}$ = +0.22 V, confirming the DFT results that the HOMO is ligand based.

The redox events in $[Et_4N]_4[\mathbf{1}]$ were further probed with spectroelectrochemistry (SEC) measurements[50] as an ideal tool for this type of systems where the ν(N═C) and ν(C═S) frequencies of the thiocyanate ligand in the infrared spectrum and ligand-based n−π^* transition in the electronic absorption spectrum act as sensitive indicators. In addition, the f−f transitions in the uranium ion can also be used to monitor changes in its oxidation state, although due to the high orbital symmetry these bands are rather weak. Spectroelectrochemistry measurements were carried out using controlled potential electrolysis in anhydrous acetonitrile containing ca. 0.1 M $[^nBu_4N][PF_6]$ at 293 K in an optically transparent thin layer electrochemical (OTTLE) cell. Changes in the IR active ν(C═N) and ν(C═S) modes in the infrared spectral profile upon application of the anodic potential of +0.22 V were examined and are shown in Figure 9. A shift of the ν(N═C) absorption band from 2047 (shown in the black line) to 2031 cm^{-1} (shown in the red line) was observed, while the ν(C═S) band at 786 cm^{-1} remained unchanged by this 1e$^-$ oxidation process. The reversibility of the initial 1e$^-$ oxidation was confirmed by the in parallel recorded thin-layer cyclic voltammogram and the parent IR spectrum reproduced upon back reduction (blue line). The corresponding UV−vis spectral changes were also examined. The 1e$^-$ oxidation of $[\mathbf{1}]^{4-}$ results in a slight wavelength shift and small decrease in the intensity of the f−f transitions (Figure S5, Supporting Information), suggesting that the oxidation state of U(IV) in $[\mathbf{1}]^{3-}$ remained unchanged. This spectroelectrochemical result has thus confirmed that the reversible anodic wave observed in the conventional and thin-layer cyclic voltammograms at +0.22 V is ligand based. The presence of a single band in the IR spectrum shifted by only 15 cm^{-1} for this oxidized product suggests that the spin density is delocalized over all thiocyanate ligands; in the largely metal-localized 1e$^-$ oxidation of a Mo(II)(NCS) complex, a shift from 2085 to 2034 cm^{-1} was observed (i.e., the M═N═C═S resonance contribution increases).[51]

In order to further probe the initial anodic process, DFT calculations were carried out on the putative one-electron-oxidized product, $[U(NCS)_8]^{3-}$. Despite not having formal D_{4d} symmetry, this complex retains approximate square-antiprismatic coordination, with U−N bond lengths between 2.365 and 2.385 Å, i.e., revealing substantial shortening on loss of an electron.[52] DFT also reproduces the red shift in the IR-active N═C stretching frequency (2044 and 2048 cm^{-1} vs 2031 cm^{-1}) observed in Figure 9, while the infrared active C═S stretching frequency does shift only slightly (831 cm^{-1}). NBO analysis supports the assignment of the 1e$^-$ oxidation as being ligand based, indicating a loss of 0.18 electrons from each NCS$^-$ ligand, primarily from S, and not from the metal. This is in agreement with the SEC data, suggesting a delocalization of the spin density over each NCS$^-$ ligand (vide supra).

The subsequent one-electron oxidation of $[Et_4N]_3[\mathbf{1}]$ in acetonitrile at +0.52 V was also investigated spectroelectrochemically (Figures 10 and 11). In the IR spectra (Figure 10) the ν(C═N) band at 2031 cm^{-1} (shown in pink) decreased in intensity and a new weak band ν(C═N) grew in at 2160 cm^{-1} (green spectrum), which matches the wavenumber reported for dithiocyanogen, NCS−SCN.[53] The electronic absorption near 320 nm most likely also belongs to this product (cf. Figure S7, Supporting Information). Back reduction of dithiocyanogen at ca. +0.30 V (corresponding to a well-defined cathodic wave in the thin-layer CV) did not recover parent $[Et_4N]_3[\mathbf{1}]$, in line with the irreversible nature of the CV response. Instead, it resulted in the appearance of a new sharp ν(C═N) band at 2063 cm^{-1} (Figure 10, black line). This could be due to formation of free $[NCS]^-$ (the S−S bond is known to be weak[54]), decomposition to form $[CN]^-$,[55] or formation of the relatively long-lived $[NCS]_2^{\bullet-}$. The UV−vis spectrum (Figure 11) shows no evidence of $[NCS]_2^{\bullet-}$ that features a characteristic absorbance at 480 nm.[28] The disappearance of the f−f transitions reflects a decomposition of the parent U(IV) complex. Moreover, the product UV−vis spectrum closely matches that of $[Et_4N]_3[UO_2(NCS)_5]$ (= $[Et_4N]_3[\mathbf{3}]$; Figure S3, Supporting Information), and this also applies for the IR ν(C═N) band shape and wavenumber of $[Et_4N]_3[\mathbf{3}]$ (Figure S9, Supporting Information) that closely resemble the ν(C═N) signature of the main product of the back reduction path of dithiocyanogen (Figure 10). It cannot be excluded, though, that a small amount of free $[NCS]^-$ (ν(C═N) at 2059/2067 cm^{-1}, Figure S6, Supporting Information) is also produced, in line with the stoichiometry of parent $[\mathbf{1}]^{4-}$ and resulting $[\mathbf{3}]^{3-}$. Remnants of moisture in the solvent or electrolyte probably supplied oxygen for the UO_2^{2+} ion

dx.doi.org/10.1021/ic501236j | Inorg. Chem. 2014, 53, 8624−8637

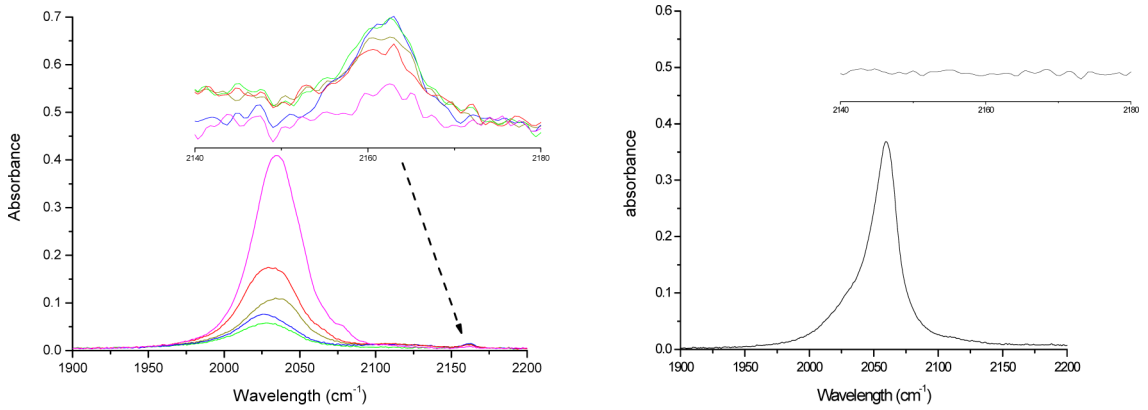

Figure 10. IR spectral changes in the ν(C═N) region accompanying the subsequent irreversible oxidation of $[Et_4N]_3[\mathbf{1}]$ at +0.52 V vs Fc/Fc$^+$ in acetonitrile/$[^nBu_4N][PF_6]$ at 293 K within an OTTLE cell. (Inset) Expanded view of the small absorption band forming at 2160 cm^{-1}. (Left) Spectral changes upon irreversible oxidation, and (right) spectrum recorded after the back reduction of $[NCS]_2$ resulting in formation of $[Et_4N]_3[UO_2(NCS)_5]$.

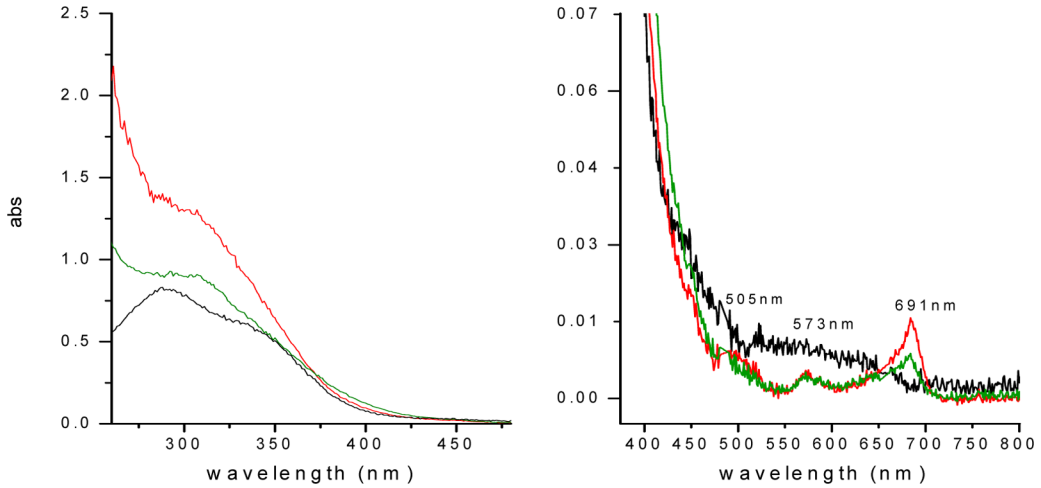

Figure 11. UV−vis spectral changes accompanying the subsequent irreversible oxidation of $[Et_4N]_3[\mathbf{1}]$ at +0.52 V vs Fc/Fc$^+$ recorded at 293 K in dry MeCN containing $[^nBu_4N][PF_6]$ within an OTTLE cell. Spectra: Red, parent $[\mathbf{1}]^{3-}$, green, after irreversible oxidation producing (among others) $(NCS)_2$ (λ_{max} = 320 nm); black, after back reduction of $(NCS)_2$ producing mainly $[Et_4N]_3[\mathbf{3}]$.

Scheme 1. Anodic and Back Reduction Paths and Respective IR ν(N═C) Wavenumbers of the Spectroelectrochemical Study of $[Et_4N]_4[\mathbf{1}]$

$$[U(NCS)_8]^{4-} \underset{}{\overset{-e^-}{\rightleftharpoons}} [U(NCS)_8]^{3-} \xrightarrow{-e^-} NCS{-}SCN \longrightarrow [UO_2(NCS)_5]^{3-}$$

ν(N=C) = 2047 cm^{-1} ν(N=C) = 2031 cm^{-1} ν(N=C) = 2160 cm^{-1} ν(N=C) = 2063 cm^{-1}

in the latter complex in the course of the intriguing irreversible oxidation of the U(IV) species $[\mathbf{1}]^{3-}$.

From the combined SEC measurements we can postulate that the 1e$^-$ oxidation of $[Et_4N]_4[\mathbf{1}]$ at +0.22 V is a reversible ligand-based oxidation process forming a ligand-centered radical species that is presumably delocalized over all NCS ligands.[56] The second 1e$^-$ oxidation process at +0.52 V is irreversible and results in formation of the dithiocyanogen, NCS−SCN. Upon back reduction the only species identifiable with certainty is the secondary uranyl product, $[Et_4N]_3[\mathbf{3}]$. This is illustrated in Scheme 1.

Structure and Spectroscopic Study of Uranyl Thiocyanate Complexes, $A_3[UO_2(NCS)_5]$. Given their potential for ionic liquid extractions, we also examined the spectroscopic properties of the uranyl(VI) thiocyanate complexes. $[Et_4N]_3[UO_2(NCS)_5]$ (= $[Et_4N]_3[\mathbf{3}]$) was prepared via the literature procedure,[26] while oxidation of $Cs_4[\mathbf{1}]$ in air allowed preparation of $Cs_3[UO_2(NCS)_5]O_{0.5}$, [**4**]; the oxygen comes from the air. The crystal structure is shown in Figure 12, and this consists of a coordination polymer whereby each $[NCS]^-$ ion shows interactions with a Cs$^+$ ion via the S atom. Additionally, the uranyl oxygen atoms participate in cation−cation interactions (CCI) with two Cs$^+$ ions to add a further dimension to polymer. CCI's have been noted previously, although there are only three other examples in the literature that display CCI's to a Cs$^+$ ion and the metric parameters are similar to those reported. The Cs$^+$ cations form long contacts with the uranyl oxygen with an average distance of 3.342 Å, agreeing reasonably well with similar Cs$^+$···O═U═O compounds.[57] The average U═O bond length is 1.768 Å, while the average U−N (2.438 Å), N═C (1.161 Å), and C═S (1.625 Å) are identical to that found in $[Et_4N]_3[\mathbf{3}]$. One manifestation of the CCI's is a reduction in the U═O bond stretching frequencies in the Raman and infrared spectra (Figure S8, Supporting Information); there is little shift compared to

dx.doi.org/10.1021/ic501236j | Inorg. Chem. 2014, 53, 8624−8637

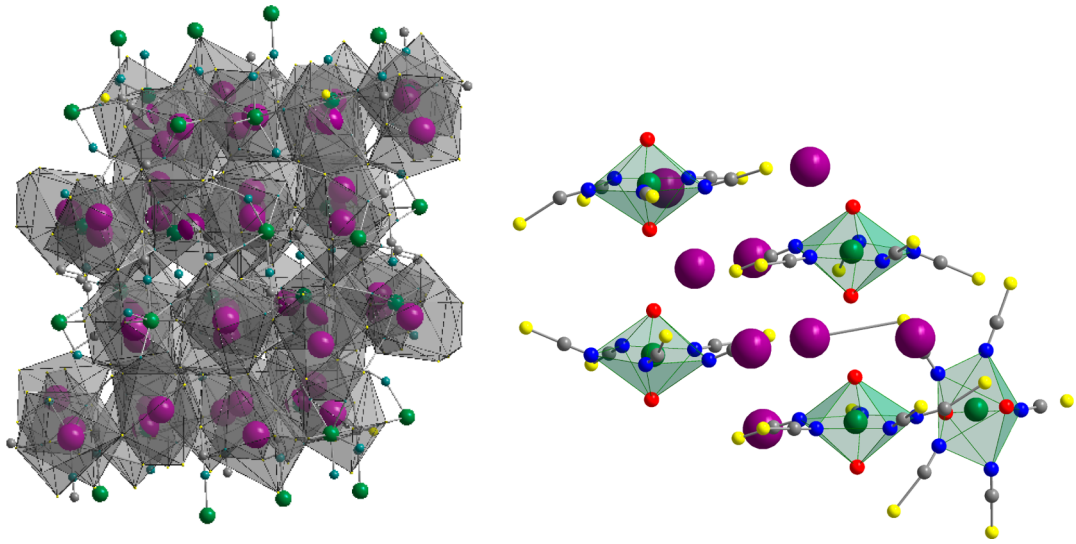

Figure 12. Solid-state structure of [**4**] showing the packing structure (left) and the uranyl coordination sphere (right) (U = green; N = blue; C = gray; S = yellow; Cs = purple; O = red).

$[Et_4N]_3[\mathbf{3}]$, suggesting that these interactions are very weak. In solution the vibrational data are identical to $[Et_4N]_3[\mathbf{3}]$, indicating that the coordination polymer is not stable.

Spectroelectrochemical Studies of $[Et_4N]_3[\mathbf{3}]$. Given the facile ligand-based 1e$^-$ oxidation of $[Et_4N]_4[\mathbf{1}]$, we were motivated to explore the redox chemistry of the uranyl thiocyanate species $[Et_4N]_3[\mathbf{3}]$. Under the same SEC conditions as described above, cyclic voltammetry of a solution of $[Et_4N]_3[\mathbf{3}]$ in acetonitrile containing 0.1 M $[^nBu_4N][BF_6]$ (Figure 13) shows an

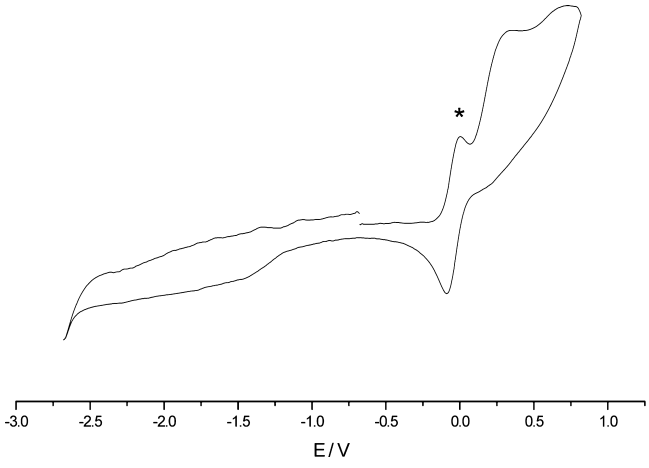

Figure 13. Cyclic voltammogram of $[Et_4N]_3[\mathbf{3}]$ in anhydrous acetonitrile/$[^nBu_4N][PF_6]$ at 298 K. Redox couple marked with the asterisk is due to the Cp_2Fe internal standard.

irreversible oxidation at +0.30 V vs (Fc/Fc^+) and an irreversible one-electron reduction at −1.45 V ascribed to the unstable $[UO_2]^{2+}/[UO_2]^+$ redox couple, in line with known formal redox potentials of U(IV)/U(V) reduction (Table 3). What is striking from this voltammogram is that the anodic and cathodic peak currents differ substantially; the internal standard redox couple is not affected. Obviously, the NCS^--based (Figure 14) oxidation of $[Et_4N]_3[\mathbf{3}]$ triggers a substantial decomposition, in contrast to $[Et_4N]_4[\mathbf{1}]$ (vide supra), and we have been unable to conclusively follow this process using spectroelectrochemistry. However, formation of dithiocyanogen was not observed.

Table 3. Formal Redox Half Potentials (vs Fc+/Fc) for the U(VI)/U(V) Couple of Selected Uranyl Complexes[a]

complex	E/V vs $[(C_5H_5)_2Fe]^{+/0}$	ref
$[Et_4N]_3[\mathbf{3}]$	−1.45	this work
$[UO_2(OH)_5]^{3-}$	−1.11	58
$[UO_2Cl_4]^{2-}$	−0.24	58
$[UO_2(salmnt^{(Et2N)2})(Py)]$	−1.81	59
$[UO_2(salen(Py)]$	−1.67	60
$[UO_2(salophen)(Py)]$	−1.63	60

[a] $salmnt^{(Et2N)2}$ = 2,3-bis[(4-diethylamino-2-hydroxobenzylidene)amino]-but-2-enedinitrile, salen = (*N*,*N*′-disalicylidene-1,2-ethylenediaminate), and salophen = (*N*,*N*′-disalicylidene-1,2-phenylenediaminate).

The 1e$^-$ reduced uranyl(V) species $[Et_4N]_4[UO_2(NCS)_5]$ would be predicted to be quite unstable as it is now quite well established that good π donors and/or sterically bulky groups in the equatorial plane are required for stabilization of this unusual oxidation state,[59,61] although there is evidence for kinetic stabilization of the $[UO_2]^+$ ion in ionic liquids.[62] Any instability would manifest itself in an irreversible reduction, and IR and UV spectra of the reduced product in the SEC measurements show only evidence of decomposition. Remarkably, the ultimate secondary reduction product identified by the IR and UV−vis absorption signatures is the U(IV) complex $[Et_4N]_4[\mathbf{1}]$ (Figure S9, Supporting Information). The mechanism of the uranyl(V) disproportionation path was not studied in detail.

DFT Calculations. Using the same functional and basis sets as for the study of $[\mathbf{1}]^{4-}$, DFT data for three uranyl compounds were calculated (Table 4), with the HOMO and LUMO of $[\mathbf{3}]^{3-}$ shown in Figure 14. NBO analysis gives σ- and π-U═O NBO's in addition to the NCS fragments as for $[\mathbf{1}]^{4-}$; these are shown in Figure S10, Supporting Information. Agreement between experiment and theory for the uranyl(VI) complex is again reasonably good for both geometry and vibrational frequencies. Bond lengths and vibrational frequencies associated with thiocyanate are generally very similar to $[\mathbf{1}]^{4-}$, while U═O data are comparable to those in previous reports. Geometric and vibrational data for the one-electron oxidation of $[\mathbf{3}]^{3-}$ are included in Table 4. From the calculations it is clear that the electron is lost from the S termini. Atoms-in-molecules analysis gives 4 charges on S of −0.684 (very similar

dx.doi.org/10.1021/ic501236j | Inorg. Chem. 2014, 53, 8624−8637

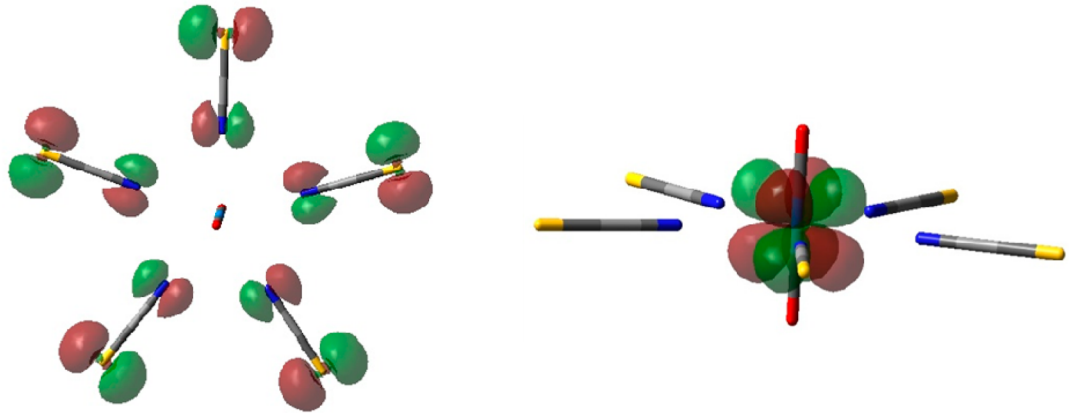

Figure 14. HOMO (left) and LUMO (right) of $[\mathbf{3}]^{3-}$ at the BP86 level of theory.

Table 4. Calculated and Experimental Bond Lengths and Vibrational Frequencies in $[\mathbf{3}]^{3-}$ and in Its 1e$^-$ Oxidized and (Calculated) Reduced Form

	bond lengths (Å)				U=O vibration (cm^{-1})		N−C vibration (cm^{-1})		C−S vibration (cm^{-1})	
	U=O	U−N	N−C	C−S	IR	Raman	IR	Raman	IR	Raman
$[\mathbf{3}]^{3-}$										
expt	1.770	2.448	1.1526	1.618	924	849	2063	2088, 2058, 2044	781	807
BP86	1.800	2.497	1.184	1.646	887	811	2076	2099	795	790
$[UO_2(NCS)_5]^{2-}$										
BP86	1.796	2.471	1.186	1.632	897	804	2034	2031	812	829
$[U^VO_2(NCS)_5]^{4-}$										
BP86	1.836	2.702	1.181	1.669	812	761	2091	2101	738	739

Table 5. Bond Critical Point Properties for Selected Compounds (values in au)[a]

compound	bond	ρ	$\nabla^2\rho$	ε	H	bond order	ref
$[UO_2(NCS)_5]^{3-}$ $[\mathbf{3}]^{3-}$	U−O	0.317	0.616	0.000	−0.302	1.893	this work
	U−N	0.047	0.188	0.066	−0.002	0.243	
	N−C	0.453	−0.497	0.006	−0.780	2.458	
	C−S	0.211	−0.260	0.004	−0.248	1.077	
$[UO_2Cl_4]^{2-}$	U−O	0.31	0.32	n.r.	n.r.	1.92	64
	U−Cl	0.05	0.12	n.r.	n.r.	0.53	
$[UO_2(NCS)_5]^{4-}$	U−O	0.286	0.484	0.000	−0.252	1.848	this work
	U−N	0.028	0.116	0.226	0.001	0.175	
	N−C	0.457	−0.424	0.000	−0.794	2.436	
	C−S	0.205	−0.372	0.003	−0.227	1.086	
$[UO_2(NCS)_5]^{2-}$	U−O	0.287	0.653	0.000	−0.243	1.948	this work
	U−N	0.052	0.206	0.052	−0.004	0.265	
	N−C	0.438	−0.550	0.017	−0.737	2.516	
	C−S	0.218	−0.278	0.021	−0.256	1.091, 1.053	
$[U(NCS)_8]^{4-}$ $[\mathbf{1}]^{4-}$	U−N	0.047	0.200	0.320	−0.007	0.219	this work
	N−C	0.445	−0.204	0.006	−0.757	2.401	
	C−S	0.215	−0.405	0.033	−0.245	1.082	
$[U(NCS)_8]^{3-}$	U−N	0.068	0.226	0.277	−0.010	0.426	this work
	N−C	0.434	−0.586	0.010	−0.730	2.516	
	C−S	0.219	−0.268	0.014	−0.260	1.094	
$[Th(NCS)_8]^{4-}$ $[\mathbf{2}]^{4-}$	Th−N	0.048	0.166	0.019	−0.002	0.243	this work
	N−C	0.444	−0.672	0.006	−0.749	2.486	
	C−S	0.216	−0.388	0.058	−0.249	1.083	
$[UCl_5(THF)]^-$	U−Cl	0.072	0.165	0.090	−0.019	0.75	15
$ThCl_4$	Th−Cl	0.081	0.157	0.011	−0.024	n.r.	63i

[a]n.r. = not reported.

to parent complex) and one +0.354, i.e., localized electron loss. In contrast, NBO analysis suggests a delocalized electron loss, with each S losing about 0.2 electrons being consistent with the delocalized nature of the HOMO. Table 4 also contains DFT predictions for the result of one-electron reduction to the uranyl(V) species. This finds significantly longer (by more than 0.2 Å) U−N

dx.doi.org/10.1021/ic501236j | Inorg. Chem. 2014, 53, 8624−8637

bonds as well as slightly longer U=O and C−S bonds, while N−C bonds are almost unaffected by the reduction. NBO analysis sheds light on these changes: charges in the uranyl(VI) and reduced complexes on U are +1.02 and +1.35, on O −0.47 and −0.65, and on NCS −0.62 and −0.82. Thus, the added electron resides mainly on O and NCS, particularly S, rather than on the metal, despite the LUMO lying on U. Moreover, the uranyl(VI) complex contains 3 U=O, 1 U−N, 3 N−C, and 1 C−S bonding orbitals, which fall to 3, 0, 3, and 1 in the reduced complex, reflecting an increased ionic character in the reduced complex.

Atoms in Molecules Analysis. Atoms-in-molecules (AIM) analysis concentrates on the topology of the electron density, giving complementary information to that from NBO, and is increasingly utilized for actinide compounds.[63] AIM analysis looks for bond critical points (BCP) between two atoms, and chemical bonding can be characterized by the properties of these BCPs. Table 5 reports properties evaluated at bond critical points for An−N and the ligand N=C and C=S bonds in a series of compounds. It is worth noting that the N=C and C=S data provide a good internal check of our calculations as they are essentially covalent. These data indicate that all compounds studied feature predominantly ionic U−N bonds, as deduced from low values of ρ, positive $\nabla^2\rho$, and energy density, H, close to zero. In contrast, U=O bonds have significant covalent character, while the expected covalency in the NCS^- ligand is reproduced, with values consistent with the resonance form found with NBO analysis. The effects of the oxidation or reduction are also evident in AIM data, for instance, in weakening U=O and U−N bonds in the uranyl species or strengthening U−N bonds on oxidation of $[\mathbf{1}]^{4-}$. Moreover, a comparison between $[\mathbf{1}]^{4-}$ and $[\mathbf{2}]^{4-}$ shows that the bonding is essentially identical, in contrast to that obtained by NBO analysis. This data also shows that a U^{IV}−NCS bond is more ionic than a U^{IV}−Cl, while for U(VI) the bonding is essentially identical.

CONCLUSIONS

The properties of the uranium(IV) thiocyanate complexes $[A]_4[U(NCS)_8]$ have been thoroughly elucidated by a number of spectroscopic and spectroelectrochemical techniques and DFT calculations. SQUID magnetic data show that the local coordination geometry can have an influence on the low-temperature magnetic susceptibility. We presented a further example of the photoluminescence spectroscopy of U(IV) compounds that suggests this technique could be a valuable probe for the electronic structure of U(IV) compounds, but the geometry of the metal center is clearly important, and high symmetry reduces the emission. Cyclic voltammetry studies show that the HOMO is ligand based, and this has been corroborated by DFT studies and spectroelectrochemical measurements. Oxidation of $Cs_4[U(NCS)_8]$ in air has allowed the isolation of an unusual coordination polymer, $Cs_3[UO_2(NCS)_5]O_{0.5}$, featuring weak cation−cation interactions between the uranyl and Cs^+ cations. $[Et_4N]_3[UO_2(NCS)_5]$ has also been studied by electrochemical and DFT methods. The oxidation and reduction couples in the CV voltammogram of this species were not studied in detail as significant decomposition occurred. However, DFT studies on the putative uranyl(V) compound have been conducted, and there is a weakening of the U−N and U=O bonds upon reduction. AIM analysis concludes that the U−N bond in all species studied is essentially ionic, but a U(IV)−Cl bond is less ionic than a U(IV)−N bond.

EXPERIMENTAL SECTION

Caution! Natural uranium was used during the course of the experimental work. In addition to the radiological hazards, uranium is a toxic metal and care should be taken with all manipulations. Experiments using uranium materials were carried out using preset radiological safety precautions in accordance with the local rules of Trinity College Dublin and the University of Reading.

All manipulations were carried out using standard Schlenk and glovebox techniques under an atmosphere of a high-purity dry argon. IR spectra were recorded on a PerkinElmer Spectrum One spectrometer with attenuated total reflectance (ATR) accessory. Raman spectra were obtained using 785 nm excitation on a Renishaw 1000 micro-Raman system in sealed capillaries. Thermal and field scans of dc and ac magnetization were carried out using a 5T Quantum Design MPMS XL SQUID magnetometer from 2 to 300 K. Powdered samples were fixed by eicosane and mounted in gel caps, which have a temperature-independent diamagnetic susceptibility, in a glovebox, and the gel caps were placed in sample straws for the measurement. Multiple measurements were taken to ensure reproducibility. Diamagnetic corrections were made using Pascal's constants.[65] Cyclic voltammetric measurements were undertaken with an AUTOLAB PGSTAT12 potentiostat/galvanostat using a platinum disc electrode with a reaction surface of 1 mm^2 as working electrode. A platinum rod electrode (together with internal referencing versus Fc/Fc^+) was used as a reference electrode and a platinum knob electrode as auxiliary electrode. All measurements took place in a glovebox under an atmosphere of high-purity nitrogen; $[^nBu_4N][BPh_4]$ (10^{-1} M) was used as electrolyte. Alternatively, in Reading, cyclic voltammetric measurements were conducted with a Metrohm Autolab PGSTAT302N potentiostat, in an airtight three-electrode cell connected to a Schlenk line, with a Pt microdisc (0.14 mm^2) working electrode, Pt coil counter electrode, and Ag coil p-reference electrode; the $[^nBu_4N][PF_6]$ electrolyte was recrystallized twice from absolute ethanol and dried under vacuum at 80 °C overnight. Controlled-potential electrolyses within the room-temperature OTTLE cell[66] were carried out using a PA4 potentiostat (Laboratory Devices, Polná, Czech Republic). IR and UV−vis spectral monitoring of the redox reactions was carried out with a Bruker Vertex 70v FT-IR spectrometer and a Scinco S3100 diode array spectrophotometer, respectively. The different redox steps were localized with the aid of contemporarily recorded thin-layer cyclic voltammograms. X-ray crystallography data were measured on a Rikagu Saturn and on a Bruker Apex diffractometer. Structures were solved by direct methods and refined on F^2 by full matrix least-squares (SHELX97) using all unique data. Crystal data, details of data collections, and refinement are given in the Supporting Information. UV−vis/NIR measurements were made on a PerkinElmer Lambda 1050 spectrophotometer over the range 300−1300 nm using fused silica cells with a path length of 1 cm. Steady-state photoluminescence spectra were recorded on a Horiba-Jobin-Yvon Fluorolog-3 spectrofluorimeter. Luminescence lifetime data were recorded following 375 and 405 nm excitation using time-correlated single-photon counting (a PCS900 plug-in PC card for fast photon counting). Lifetimes were obtained by tail fit on the data obtained, and the quality of fit was judged by minimization of reduced chi-squared and residuals squared.

THF was distilled over potassium or Na/benzophenone, while acetonitrile and CD_3CN were distilled over CaH_2 or P_2O_5 and degassed immediately prior to use. Spectroscopic measurements used spectroscopic-grade solvents which were purchased from commercial sources, dried over molecular sieves, and thoroughly degassed before use. $[Et_4N]_4[U(NCS)_8]$, $[Et_4N]_4[Th(NCS)_8]$,[18b] and $[Et_4N]_3[UO_2(NCS)_5]$[26] were made via the literature procedures, while all other reagents were obtained from commercial sources.

Synthesis of $[Bu_4N]_4[U(NCS)_8]\cdot 2MeCN$. To a suspension of UCl_4 (100 mg, 0.25 mmol) in acetonitrile (20 cm^3) was added Na[NCS] (170.75 mg, 2.11 mmol) and $^nBu_4NCl$ (291.82 mg, 1.05 mmol). The mixture was stirred at room temperature for 30 min. The resulting green solution was filtered, and the solvent was reduced in volume. Placement at −20 °C overnight yielded dark green crystals suitable for X-ray diffraction (240 mg, 0.16 mmol, 64%). IR (cm^{-1}): 2047, 2090 ν(CN),

dx.doi.org/10.1021/ic501236j | Inorg. Chem. 2014, 53, 8624−8637

783 ν(CS). Raman (cm^{-1}): 2090, 2056, and 2045 ν(CN), 796 ν(CS). UV−vis−NIR (ε mol dm^{-3} cm^{-1}): (MeCN, ~10^{-4} M) 230 (12833.4), 475 (33.8), 505 (87.8), 573 (32.5), 691 (214), 933 (35), 1168 (127), 1584 (65), 1994 nm (25).

Synthesis of $Cs_3[UO_2(NCS)_5]\cdot O_{0.5}$. A solution of $Cs_4[U(NCS)_8]$ in acetonitrile was left to stand in air at room temperature. After 2 weeks dark yellow crystals suitable for X-ray diffractions were collected. IR (cm^{-1}): 2104, 2020 ν(CN), 900 ν(UO), 798 ν(CS); Raman (cm^{-1}): 2095, 2060, 2040 ν(CN), 849 ν(UO), 821 ν(CS); Anal. Calcd for $Cs_3UO_{2.5}N_5C_5S_5$: C, 6.21; N, 7.24. Found: C, 6.13; N, 7.27.

COMPUTATIONAL DETAILS

DFT geometry optimization was performed on single molecules, extracted from the crystal structure, at the unrestricted BP86/def2-TZVP[67,68] level using Turbomole[69] initially without symmetry constraints but subsequently in D_{4d} or D_{5h} point groups, as appropriate. Scalar relativistic effects in uranium were included through the use of effective core potentials, as defined for this basis set. Spin contamination was not significant, with values of S^2 within 1% of the anticipated value of 2.00. Further single-point DFT calculations were performed in Gaussian09[70] using the BP86 and B3LYP[71] functionals. The (27 s 24p 18d 14f 6 g)/[8s 7p 5d 3f 1g] all-electron ANO-RCC basis sets of DZP quality were used for uranium,[72] with 6-31+G(d,p) on C, O, H, and Cl.[73] Scalar relativistic effects were included via the second-order Douglas−Kroll−Hess Hamiltonian.[74] Natural bond orbital (NBO) analysis[75] was performed using Gaussian09; atoms-in-molecules (AIM) analysis used AIMAll.[76] Topological analysis of the electronic density (ρ) is based upon those points where the gradient of the density, $\nabla\rho$, vanishes.[77] In this work we consider points where one curvature (in the internuclear direction) is positive and two (perpendicular to the bond direction) are negative, termed (3, −1) or bond critical points. Properties evaluated at such points characterize the bonding interactions present. The second derivative of ρ or Laplacian, $\nabla^2\rho$, and the bond ellipticity, the ratio of the two negative curvatures, are reported, as is the local energy density, H, defined as the sum of the kinetic and potential energy densities. An electron density (ρ) of 0.2 au or greater typically signifies a covalent bond, and less than 0.1 au indicates closed shell (ionic, van der Waals, etc.). The Laplacian of this function ($\nabla^2\rho$) is typically significantly negative for covalent bonding and positive for closed shell interactions. The ellipticity, ε, measures the shape of the electron density distribution in a plane through the BCP and thus determines the degree of cylindrical symmetry in a bond. H is the total energy density (kinetic + potential energies) and is typically negative for covalent bonds. This reveals whether accumulation of electronic density is stabilizing ($E < 0$) or destabilizing ($E > 0$). Integrated properties of atoms were checked for numerical accuracy via the basin integral of the Laplacian, which should vanish for properly defined atomic basins (all values 10^{-4} or less), and also by comparison of the sum of all atomic integrals with directly calculated molecular values. Integration of the overlap matrix over atomic basins can be used to derive covalent bond order, as set out by Angyan et al.[78]

ASSOCIATED CONTENT

Supporting Information

Structural data for orange $[Et_4N][U(NCS)_8]$, variable field and ac susceptibility plots for Cs_4[**1**] and $[Et_4N]_4$[**1**], UV−vis absorption spectrum and spectroelectrochemical study of $[Et_4N]_3$[**3**], CV of $[Et_4N]_4$[**1**] in acetonitrile, Raman spectra of [**4**], IR/UV−vis spectroelectrochemical study of Na[NCS] in acetonitrile, and further computational details. This material is available free of charge via the Internet at http://pubs.acs.org. CCDC 988009−988010 contains the supplementary crystallographic data for this paper. These data can be obtained free of charge from The Cambridge Crystallographic Data Centre via www.ccdc.cam.ac.uk/data_request/cif.

AUTHOR INFORMATION

Corresponding Author

*Phone: +353-1-8963501. Fax: +353-1-6712826. E-mail: Bakerrj@tcd.ie.

Author Contributions

The manuscript was written through contributions of all authors. All authors have given approval to the final version of the manuscript.

Notes

The authors declare no competing financial interest.

ACKNOWLEDGMENTS

We thank TCD (R.J.B. and E.H.) for funding this work. J.A.P. is grateful to UK National Service for Computational Chemistry Software. F.H. thanks the University of Reading (SCFP) for logistic support of the Spectroelectrochemistry Laboratory. M.E. and G.L. thank MINECO (MAT2012-38318-C03). We thank Professor Damien Murphy (Cardiff University) for the EPR measurements.

REFERENCES

(1) (a) Hayton, T. W. *Chem. Commun.* **2013**, *49*, 2956−2973. (b) La Pierre, H. S.; Meyer, K. *Inorg. Chem.* **2013**, *52*, 529−539. (c) Jones, M. B.; Gaunt, A. J. *Chem. Rev.* **2013**, *113*, 1137−1198. (d) Hayton, T. W. *Dalton Trans.* **2010**, *39*, 1145−1158. (e) Liddle, S. T.; Mills, D. P. *Dalton Trans.* **2009**, 5592−5605. (e) Liddle, S. T. *Proc. R. Soc. A* **2009**, *465*, 1673−1700. (f) Castro-Rodríguez, I.; Meyer, K. *Chem. Commun.* **2006**, 1353−1368. (g) Ephritikhine, M. *Dalton Trans.* **2006**, 2501−2516.

(2) (a) La Pierre, H. S.; Heinemann, F. W.; Meyer, K. *Chem. Commun.* **2014**, *50*, 3962−3964. (b) Baker, R. J. *Coord. Chem. Rev.* **2012**, *256*, 2843−2871.

(3) Gardner, B. M.; Liddle, S. T. *Eur. J. Inorg. Chem.* **2013**, 3753−3770.

(4) For reviews see: (a) Graves, C. R.; Kiplinger, J. L. *Chem. Commun.* **2009**, 3831−3853. (b) Arnold, P. L.; Love, J. B.; Patel, D. *Coord. Chem. Rev.* **2009**, *253*, 1973−1978.

(5) Baker, R. J. *Chem.—Eur. J.* **2012**, *18*, 16258−16271.

(6) MacDonald, M. R.; Fieser, M. E.; Bates, J. E.; Ziller, J. W.; Furche, F.; Evans, W. J. *J. Am. Chem. Soc.* **2013**, *135*, 13310−13313.

(7) La Pierre, H. S.; Scheurer, A.; Heinemann, F. W.; Hieringer, W.; Meyer, K. *Angew. Chem., Int. Ed.* **2014**, *53*, 7158−7162.

(8) King, D. M.; Tuna, F.; McInnes, E. J. L.; McMaster, J.; Lewis, W.; Blake, A. J.; Liddle, S. T. *Science* **2012**, *337*, 717−720.

(9) King, D. M.; Tuna, F.; McInnes, E. J. L.; McMaster, J.; Lewis, W.; Blake, A. J.; Liddle, S. T. *Nat. Chem.* **2013**, *5*, 482−488.

(10) For recent reviews, see: (a) Kaltsoyannis, N. *Inorg. Chem.* **2013**, *52*, 3407−3413. (b) Neidig, M. L.; Clark, D. L.; Martin, R. L. *Coord. Chem. Rev.* **2013**, *257*, 394−406.

(11) Takao, K.; Bell, T. J.; Ikeda, Y. *Inorg. Chem.* **2013**, *52*, 3459−72.

(12) (a) Natrajan, L. S. *Coord. Chem. Rev.* **2012**, *256*, 1583−1603. (b) Billard, I.; Geipel, G. *Springer Ser. Fluoresc.* **2008**, *5*, 465−492. (c) Burrows, H. D.; Miguel, M. D. G. *Adv. Colloid Interface Sci.* **2001**, *89−90*, 485−496. (d) Baird, C. P.; Kemp, T. J. *Prog. React. Kinet.* **1997**, *22*, 87−139. (e) Denning, R. G. *J. Phys. Chem. A* **2007**, *111*, 4125−4143.

(13) (a) Redmond, M. P.; Cornet, S. M.; Woodall, S. D.; Whittaker, D.; Collison, D.; Helliwell, M.; Natrajan, L. S. *Dalton Trans.* **2011**, *40*, 3914−3926. (b) Hashem, E.; McCabe, T.; Schulzke, C.; Baker, R. J. *Dalton Trans.* **2014**, *43*, 1125−1131.

(14) (a) Geipel, G. *Coord. Chem. Rev.* **2006**, *250*, 844−854. (b) Liu, G.; Beitz, J. V. In *The Chemistry of the Actinide and Transactinide Elements*; Morss, L. R., Edelstein, N. M., and Fuger, J., Eds.; Springer: Dordrecht, The Netherlands, 2010. (c) Girnt, D.; Roesky, P. W.; Geist, A.; Ruff, C. M.; Panak, P. J.; Denecke, M. A. *Inorg. Chem.* **2010**, *49*, 9627−9635.

(15) (a) Hashem, E.; Swinburne, A. N.; Schulzke, C.; Evans, R. C.; Platts, J. A.; Kerridge, A.; Natrajan, L. S.; Baker, R. J. *RSC Adv.* **2013**, *3*, 4350−4361. (b) Hashem, E.; Lorusso, G.; Evangelisti, M.; McCabe, T.;

Schulzke, C.; Platts, J. A.; Baker, R. J. *Dalton Trans.* **2013**, *42*, 14677−14680.
(16) (a) Kirishima, A.; Kimura, T.; Tochiyama, O.; Yoshida, Z. *Chem. Commun.* **2003**, 910−911. (b) Kirishima, A.; Kimura, T.; Nagaishi, R.; Tochiyama, O. *Radiochim. Acta* **2004**, *92*, 705−710.
(17) Danilo, C.; Vallet, V.; Flament, J.-P.; Wahlgren, U. *Phys. Chem. Chem. Phys.* **2010**, *12*, 1116−1130.
(18) (a) Arutyunyan, E. G.; Porai-Koshits, M. A. *Zh. Struk. Khim.* **1963**, *4*, 110−111. (b) Bagnall, K. W.; Brown, D.; Colton, R. *J. Chem. Soc.* **1964**, 2527−2530.
(19) (a) Countryman, R.; McDonald, W. S. *J. Inorg. Nucl. Chem.* **1971**, *33*, 2213−2220. (b) Al-Kazzaz, Z. M. S.; Bagnall, K. W.; Brown, D.; Whittaker, B. *J. Chem. Soc., Dalton Trans.* **1972**, 2273−2237.
(20) Bombieri, G.; Moseley, P. T.; Brown, D. *J. Chem. Soc., Dalton Trans.* **1975**, 1520−1523.
(21) (a) Griffith, W. P.; Mockford, M. J. *J. Chem. Soc., Dalton Trans.* **1986**, 1057−1058. (b) Grey, I. E.; Smith, P. W. *Aus. J. Chem.* **1969**, *22*, 311−315.
(22) (a) Borkowski, M.; Lis, S.; Siekierski, S. *J. Alloys Compd.* **1998**, *275*−*277*, 754−758. (b) Borkowski, M.; Krejzler, J.; Siekierski, S. *Radiochim. Acta* **1994**, *65*, 99. (c) Khopkar, P. K.; Mathur, J. N. *J. Inorg. Nucl. Chem.* **1980**, *42*, 109−113. (d) Chiarizia, R.; Danesi, P. R.; Scibona, G.; Magon, L. *J. Inorg. Nucl. Chem.* **1973**, *35*, 3595−3604. (e) Moore, F. L. *Anal. Chem.* **1964**, *36*, 2158−2162.
(23) Srncik, M.; Kogelnig, D.; Stojanovic, A.; Korner, W.; Krachler, R.; Wallner, G. *Appl. Radiat. Isot.* **2009**, *67*, 2146−2149.
(24) (a) Alcock, N. W.; Roberts, M. M.; Brown, D. *Acta Crystallogr.* **1982**, *B38*, 2870−2872. (b) Bombieri, G.; Forsellini, E.; Graziani, R.; Pappalardo, G. C. *Transition Met. Chem.* **1979**, *4*, 70−72. (c) Vdovenko, V. M.; Skoblo, A. I.; Suglobov, D. N. *Radiokhimiya* **1967**, *9*, 119−123.
(25) Aoyagi, N.; Shimojo, K.; Brooks, N. R.; Nagaishi, R.; Naganawa, H.; Van Hecke, K.; Van Meervelt, L.; Binnemans, K.; Kimura, T. *Chem. Commun.* **2011**, *47*, 4490−4492.
(26) Rowland, C. E.; Kanatzidis, M. G.; Soderholm, L. *Inorg. Chem.* **2012**, *51*, 11798−11804.
(27) Charpin, P.; Costes, R. M.; Folcher, G.; Plurien, P.; Navaza, A.; de Rango, C. *Inorg. Nucl. Chem. Lett.* **1977**, *13*, 341−347.
(28) (a) Michalski, R.; Sikora, A.; Adamus, J.; Marcinek, A. *J. Phys. Chem. A* **2010**, *114*, 861−866. (b) Mainusch, B.; Karocki, A.; Guldi, D. M.; Stasicka, Z.; Wasgestian, F. *Inorg. Chim. Acta* **1997**, *255*, 87−93. (c) Kirk, A. D.; Cai, L.-Z. *Inorg. Chem.* **1995**, *34*, 3986−3992. (d) Nord, G.; Pedersen, B.; Floryan-Løvborg, E.; Pagsberg, P. *Inorg. Chem.* **1982**, *21*, 2327−2330.
(29) Refinement of the structure with an S-bound thiocyanate ligand results in a substantial worsening of the *R* factor and displacement factors for S.
(30) Reinhart, J. D.; Long, J. R. *Chem. Sci.* **2011**, *2*, 2078−2085.
(31) Rinehart, J. D.; Long, J. R. *J. Am. Chem. Soc.* **2009**, *131*, 12558−12559.
(32) Rinehart, J. D.; Meihaus, K. R.; Long, J. R. *J. Am. Chem. Soc.* **2010**, *132*, 7572−7573.
(33) Rinehart, J. D.; Long, J. R. *Dalton Trans.* **2012**, *41*, 13572−13574.
(34) (a) Antunes, M. A.; Santos, I. C.; Bolvin, H.; Pereira, L. C. J.; Mazzanti, M.; Marçalo, J.; Almeida, M. *Dalton Trans.* **2013**, *42*, 8861−8867. (b) Coutinho, J. T.; Antunes, M. A.; Pereira, L. C. J.; Bolvin, H.; Marçalo, J.; Mazzanti, M.; Almeida, M. *Dalton Trans.* **2012**, *41*, 13568−13571.
(35) Antunes, M. A.; Pereira, L. C. J.; Santos, I. C.; Mazzanti, M.; Marçalo, J.; Almeida, M. *Inorg. Chem.* **2011**, *50*, 9915−9917.
(36) Mills, D. P.; Moro, F.; McMaster, J.; van Slageren, J.; Lewis, W.; Blake, A. J.; Liddle, S. T. *Nat. Chem.* **2011**, *3*, 454−460.
(37) Mougel, V.; Chatelain, L.; Pecaut, J.; Caciuffo, R.; Colineau, E.; Griveau, J.-C.; Mazzanti, M. *Nat. Chem.* **2012**, *4*, 1011−1017.
(38) Moro, F.; Mills, D. P.; Liddle, S. T.; van Slageren, J. *Angew. Chem., Int. Ed.* **2013**, *52*, 3430−3433.
(39) King, D. M.; Tuna, F.; McMaster, J.; Lewis, W.; Blake, A. J.; McInnes, E. J. L.; Liddle, S. T. *Angew. Chem., Int. Ed.* **2013**, *52*, 4921−4924.
(40) Mougel, V.; Chatelain, L.; Hermle, J.; Caciuffo, R.; Colineau, E.; Tuna, F.; Magnani, N.; de Geyer, A.; Pecaut, J.; Mazzanti, M. *Angew. Chem., Int. Ed.* **2014**, *53*, 819−823.
(41) Baldoví, J. J.; Cardona-Serra, S.; Clemente-Juan, J. M.; Coronado, E.; Gaita-Arino, A. *Chem. Sci.* **2013**, *4*, 938−946.
(42) Photoluminescence from $[Th(PO_3C_6H_4CO_2H)F_2]$ has been reported, but these arise from the ligand. Adelani, P. O.; Albrecht-Schmitt, T. E. *Inorg. Chem.* **2010**, *49*, 5701−5705.
(43) Hilton, D. J.; Prasankumar, R. P.; Schelter, E. J.; Thorsmolle, V. K.; Trugman, S. A.; Shreve, A. P.; Kiplinger, J. L.; Morris, D. E.; Taylor, A. J. *J. Phys. Chem. A* **2008**, *112*, 7840−7847.
(44) For recent reviews, see: (a) Wang, D.; van Gunsteren, W. F.; Chai, Z. *Chem. Soc. Rev.* **2012**, *41*, 5836−5865. (b) Kirker, I.; Kaltsoyannis, N. *Dalton Trans.* **2011**, *40*, 124−131. (c) Schreckenbach, G.; Shamov, G. A. *Acc. Chem. Res.* **2010**, *43*, 19−29. (d) Tassell, M. J.; Kaltsoyannis, N. *Dalton Trans.* **2010**, *39*, 6719−6725. (e) Gagliardi, L.; Roos, B. O. *Chem. Soc. Rev.* **2007**, *36*, 893−903. (f) Kaltsoyannis, N. *Chem. Soc. Rev.* **2003**, *32*, 9−16.
(45) Vibrational frequencies have not been scaled, since recommended scaling factors are not available for the specific combination of functional and basis set used here. However, typical scaling factors for basis sets of similar size to those used here with BLYP (0.995) and B3LYP (0.970), obtained from http://cccbdb.nist.gov/would, not change the overall conclusions reached and would bring BP86 data into slightly better agreement with experiment.
(46) (a) Ohaion, T.; Kalisky, Y.; Ben-Eliyahu, Y.; Becker, J. Y.; Bettelheim, A. *Eur. J. Inorg. Chem.* **2013**, 3477−3482. (b) Vicente, J.; Diaz, M. *Environ. Sci. Technol.* **2003**, *37*, 1452−1456.
(47) (a) Sonnenberger, D. C.; Gaudiello, J. G. *Inorg. Chem.* **1988**, *27*, 2747−2748. (b) Finke, R. G.; Gaughan, G.; Voegeli, R. *J. Organomet. Chem.* **1982**, *229*, 179−184.
(48) Clappe, C.; Leveugle, D.; Hauchard, D.; Durand, G. *J. Electroanal. Chem.* **1998**, *448*, 95−103.
(49) Morris, D. E.; DaRe, R. E.; Jantunen, K. C.; Castro-Rodríguez, I.; Kiplinger, J. L. *Organometallics* **2004**, *23*, 5142−5153.
(50) Kaim, W.; Fiedler, J. *Chem. Soc. Rev.* **2009**, *38*, 3373−3382.
(51) Tory, J.; Gobaille-Shaw, G.; Chippindale, A. M.; Hartl, F. *J. Organomet. Chem.* **2014**, *760*, 30−41.
(52) It is worth noting that this corroborates our assessment of the orange photoproduct that has been structurally characterized, i.e., it is not a photo-oxidized species as the shorter bond lengths are not observed in the X-ray structure (Tables S1−S3, Supporting Information).
(53) (a) Burchell, C. J.; Kilian, P.; Slawin, A. M. Z.; Woollins, J. D. *Inorg. Chem.* **2006**, *45*, 710−716. (b) Devore, T. C. *J. Mol. Struct.* **1987**, *162*, 287−304. (c) Vanderzee, C. E.; Quist, A. S. *Inorg. Chem.* **1966**, *5*, 1238−1242.
(54) Jensen, J. O. *J. Mol. Struct.: THEOCHEM* **2005**, *714*, 137−141.
(55) Cataldo, F. *Polyhedron* **2000**, *19*, 681−688.
(56) Coordinated NCS radicals to transition metals have been reported: Losada, J.; Morán, M. *J. Organomet. Chem.* **1984**, *276*, 13−19.
(57) (a) Adelani, P. O.; Oliver, A. G.; Albrecht-Schmitt, T. E. *Crys. Growth. Des.* **2011**, *11*, 3072−3080. (b) Locock, A. J.; Burns, P. C. *J. Solid. State. Chem.* **2003**, *175*, 372−379. (c) Thuéry, P.; Masci, B. *Dalton Trans.* **2003**, 2411−2417.
(58) Morris, D. E. *Inorg. Chem.* **2002**, *41*, 3542−3547.
(59) Hardwick, H. C.; Royal, D. S.; Helliwell, M.; Pope, S. J. A.; Ashton, L.; Goodacre, R.; Sharrad, C. A. *Dalton Trans.* **2011**, *40*, 5939−5952.
(60) Kim, S.-Y.; Tomiyasu, H.; Ikeda, Y. *J. Nucl. Sci. Technol.* **2002**, *39*, 160−165.
(61) Clark, D. L.; Conradson, S. D.; Donohoe, R. J.; Keogh, D. W.; Morris, D. E.; Palmer, P. D.; Rogers, R. D.; Tait, C. D. *Inorg. Chem.* **1999**, *38*, 1456−1466.
(62) For recent examples see: (a) Yaprak, D.; Spielberg, E. T.; Bäcker, T.; Richter, M.; Mallick, B.; Klein, A.; Mudring, A.-V. *Chem.—Eur. J.* **2014**, *20*, 6482−6493. (b) Ogura, T.; Takao, K.; Sasaki, K.; Arai, T.; Ikeda, Y. *Inorg. Chem.* **2011**, *50*, 10525−10527. (c) Ikeda, Y.; Hiroe, K.; Asanuma, N.; Shirai, A. *J. Nucl. Sci. Technol.* **2009**, *46*, 158−162.

(63) Selected examples where AIM has been extensively utilized: (a) Lu, E.; Cooper, O. J.; McMaster, J.; Tuna, F.; McInnes, E. J. L.; Lewis, W.; Blake, A. J.; Liddle, S. T. *Angew. Chem., Int. Ed.* **2014**, *53*, 6696−6700. (b) Mountain, A. R. E.; Kaltsoyannis, N. *Dalton Trans.* **2013**, *42*, 13477−13486. (c) Brown, J. L.; Fortier, S.; Wu, G.; Kaltsoyannis, N.; Hayton, T. W. *J. Am. Chem. Soc.* **2013**, *135*, 5352−5355. (d) Kaltsoyannis, N. *Inorg. Chem.* **2013**, *52*, 3407−3413. (e) Mills, D. P.; Cooper, O. J.; Tuna, F.; McInnes, E. J. L.; Davies, E. S.; McMaster, J.; Moro, F.; Lewis, W.; Blake, A. J.; Liddle, S. T. *J. Am. Chem. Soc.* **2012**, *134*, 10047−10054. (f) Gardner, B. M.; Patel, D.; Cornish, A. D.; McMaster, J.; Lewis, W.; Blake, A. J.; Liddle, S. T. *Chem.—Eur. J.* **2011**, *17*, 11266−11273. (g) Vlaisavljevich, B.; Miro, P.; Cramer, C. J.; Gagliardi, L.; Infante, I.; Liddle, S. T. *Chem.—Eur. J.* **2011**, *17*, 8424−8433. (h) Kirker, I.; Kaltsoyannis, N. *Dalton Trans.* **2011**, *40*, 124−131. (i) Tassell, M. J.; Kaltsoyannis, N. *Dalton Trans.* **2010**, *39*, 6719−6725. (j) Arnold, P. L.; Turner, Z. R.; Kaltsoyannis, N.; Pelekanaki, P.; Bellabarba, R. M.; Tooze, R. P. *Chem.—Eur. J.* **2010**, *16*, 9623−9629. (k) Petit, L.; Joubert, L.; Maldivi, P.; Adamo, C. *J. Am. Chem. Soc.* **2006**, *128*, 2190−2191. (l) Clark, A. E.; Sonnenberg, J. L.; Hay, P. J.; Martin, R. L. *J. Chem. Phys.* **2004**, *121*, 2563−2570.

(64) Vallet, V.; Wahlgren, U.; Grenthe, I. *J. Phys. Chem. A* **2012**, *116*, 12373−12380.

(65) Bain, G. A.; Berry, J. F. *J. Chem. Educ.* **2008**, *85*, 532−536.

(66) Krejčík, M.; Daněk, M.; Hartl, F. *J. Electroanal. Chem.* **1991**, *317*, 179−187.

(67) (a) Becke, A. D. *Phys. Rev. A* **1988**, *38*, 3098−3100. (b) Perdew, J. P. *Phys. Rev. B* **1986**, *33*, 8822−8824.

(68) Weigend, F.; Ahlrichs, R. *Phys. Chem. Chem. Phys.* **2005**, *7*, 3297−3305.

(69) Turbomole v5.10: Ahlrichs, R.; Baer, M.; Haeser, M.; Horn, H.; Koelmel, C. *Chem. Phys. Lett.* **1989**, *162*, 165−169.

(70) Frisch, M. J.; Trucks, G. W.; Schlegel, H. B.; Scuseria, G. E.; Robb, M. A.; Cheeseman, J. R.; Scalmani, G.; Barone, V.; Mennucci, B.; Petersson, G. A.; Nakatsuji, H.; Caricato, M.; Li, X.; Hratchian, H. P.; Izmaylov, A. F.; Bloino, J.; Zheng, G.; Sonnenberg, J. L.; Hada, M.; Ehara, M.; Toyota, K.; Fukuda, R.; Hasegawa, J.; Ishida, M.; Nakajima, T.; Honda, Y.; Kitao, O.; Nakai, H.; Vreven, T.; Montgomery, J. A.; , Jr., Peralta, J. E.; Ogliaro, F.; Bearpark, M.; Heyd, J. J.; Brothers, E.; Kudin, K. N.; Staroverov, V. N.; Keith, T.; Kobayashi, R.; Normand, J.; Raghavachari, K.; Rendell, A.; Burant, J. C.; Iyengar, S. S.; Tomasi, J.; Cossi, M.; Rega, N.; Millam, J. M.; Klene, M.; Knox, J. E.; Cross, J. B.; Bakken, V.; Adamo, C.; Jaramillo, J.; Gomperts, R.; Stratmann, R. E.; Yazyev, O.; Austin, A. J.; Cammi, R.; Pomelli, C.; Ochterski, J. W.; Martin, R. L.; Morokuma, K.; Zakrzewski, V. G.; Voth, G. A.; Salvador, P.; Dannenberg, J. J.; Dapprich, S.; Daniels, A. D.; Farkas, O.; Foresman, J. B.; Ortiz, J. V.; Cioslowski, J.; Fox, D. J. *Gaussian 09*, Revision B.01; Gaussian, Inc.: Wallingford, CT, 2010.

(71) (a) Becke, A. D. *J. Chem. Phys.* **1993**, *98*, 5648−5652. (b) Lee, C.; Yang, W.; Parr, R. G. *Phys. Rev. B* **1988**, *37*, 785−789.

(72) Roos, B. O.; Lindh, R.; Malmqvist, P.-Å.; Veryazov, V.; Widmark, P.-O. *J. Phys. Chem. A* **2008**, *112*, 11431−11435.

(73) (a) Hehre, W. J.; Ditchfield, R.; Pople, J. A. *J. Chem. Phys.* **1972**, *56*, 2257−2261. (b) Clark, T.; Chandrasekhar, J.; Spitznagel, G. W.; Schleyer, P. V. R. *J. Comput. Chem.* **1983**, *4*, 294−301. (c) Hariharan, P. C.; Pople, J. A. *Theor. Chim. Acta* **1973**, *28*, 213−222.

(74) Jansen, G.; Hess, B. A. *Phys. Rev. A* **1989**, *39*, 6016−6017 and references cited therein.

(75) Reed, A. E.; Weinhold, F. *J. Chem. Phys.* **1985**, *83*, 1736−1740.

(76) Keith, T. AIMAll http://aim.tkgristmill.com.

(77) Bader, R. F. W. *Atoms in Molecules-A Quantum Theory*; Oxford University Press: Oxford, 1990.

(78) Kar, T.; Angyan, J. G.; Sannigrahi, A. B. *J. Phys. Chem. A* **2000**, *104*, 9953−9963.